THE AMERICAN MINERALOGIST

JOURNAL OF THE MINERALOGICAL SOCIETY OF AMERICA

Vol. 30 NOVEMBER–DECEMBER, 1945 Nos. 11 and 12

SOME OBSERVATIONS ON THE OPTICAL PROPERTIES OF LONG CHAIN NORMAL PARAFFINS

BELA HUBBARD, *Mount Vernon, New York*

ABSTRACT

This paper presents the results of optical studies of the crystals of long chain normal paraffins. The studies were restricted to crystals grown from solvent solution at ordinary temperatures; polymorphic crystal forms obtained under other conditions are not considered.

It is shown that all long chain *n*-paraffin crystals, including very pure synthetic compounds and those occurring in nature, are optically active and invariably dextrorotatory. It is further shown that the crystals are normally orthorhombic, approaching hexagonal symmetry. No monoclinic crystals have been found.

The cause of the optical activity is discussed. The writer holds that the zig-zag type of molecular chain, currently believed to exist in the long chain *n*-paraffins, cannot cause the observed optical activity. A spiral molecular chain for these compounds is proposed as a working theory. Such a spiral chain is believed to account for the observed optical rotation.

INTRODUCTORY STATEMENT

The present paper deals with the crystal structure of normal paraffins within the wax range: that is, the homologous series of *n*-paraffins above $C_{15}H_{32}$, which are waxy solids at ordinary temperatures. The observations here summarized, and which are the basis of the paper, were made on *n*-paraffin crystals ranging from C_{21} to C_{32}, inclusive. These were crystallized on glass microslides from a solvent solution at ordinary temperatures, between 20°C. and 25°C. The crystals studied ranged from very pure individual *n*-paraffins to mixtures of two or three *n*-paraffins differing by one or a few carbon atoms. All materials studied were "pure" to the extent that non-paraffin impurities were absent, or present in such small quantities as not to affect materially the crystallization.

All optical observations were made with a petrographic microscope, and except where stated otherwise, were made at ordinary air temperatures. The light source was a 10 watt lamp with Corning "Daylight" filter. Observations and measurements of crystals using controlled higher-than-ordinary temperatures were made with a Leitz-Weygand heating stage, the temperatures being estimated to the nearest 0.1°C. with a probable error in most observations of ±0.2°C. Crystal interfacial angles were determined by averaging at least five readings, the probable error of a single reading being about ±0.12°, and of the mean, about ±0.05°.

The primary objective of this paper is to present the results of the writer's microscopic observations of *n*-paraffin crystals and his interpretation of the molecular and crystalline structures of the long chain normal paraffin series, based on these observations. These studies have been carried out intermittently over a period of four years, and have involved the preparation and examination of more than two thousand microslides of paraffin waxes from ninety five different sources. It is the writer's belief that the results of these studies are worth recording, if only to attempt to clear up some of the apparently contradictory observations to be found in an extensive literature on the subject. Furthermore, certain optical properties of *n*-paraffins described in the present paper are difficult if not impossible to explain if the molecule of the long chain *n*-paraffin has the generally accepted zig-zag form, as interpreted from *x*-ray studies.

To prevent possible misunderstanding, it is emphasized that the *n*-paraffin crystals described in this paper are exclusively those grown on a glass microslide from a solvent solution (carbon tetrachloride, benzene, toluene, or xylene) at ordinary temperatures well below the melting points. The same compounds, crystallized under different conditions, show quite different crystalline forms. This fact is largely responsible for the confusion one finds in reviewing the many published descriptions of paraffin crystals. The present paper does not attempt to cover the subject of polymorphism in *n*-paraffin crystals, or the causes thereof.

EXTERNAL CRYSTAL FORM OF NORMAL PARAFFIN

The form and optical orientation of the typical *n*-paraffin crystal are shown in Fig. 1. The crystallization is generally orthorhombic, but ranges from orthorhombic to hexagonal. In the common form the pinacoid {001} and the rhombic prism {110} predominate. The pinacoid {010} is occasionally developed. The pinacoid {100} occurs rarely, but has not been observed where the pinacoid {010} is developed.

The crystals are small. The long, or *b*-axis direction of the rhombic plate rarely is found to exceed 0.7 mm., and the usual length for the larger crystals on the average slide is from 0.1 mm. to 0.5 mm. The average thickness, in the *c*-axis direction, is of the order of 0.005 to 0.01 mm.

Euhedral crystals of a very pure[1] *n*-paraffin are nearly perfect in form, the corresponding interfacial angles in all crystals being nearly the same. Mix crystals of two or more *n*-paraffins, or crystals of a single *n*-paraffin containing impurities, are generally more or less distorted and show considerable variation in interfacial angles, both within the same crystal and among different crystals in a single preparation.

---

[1] Normal paraffin wax compounds of 100% purity probably do not exist. Paraffins graded as "c.p." may contain up to several per cent of other members of the same homologous series. The term "very pure" as used throughout this paper indicates a compound probably at least 98% pure.

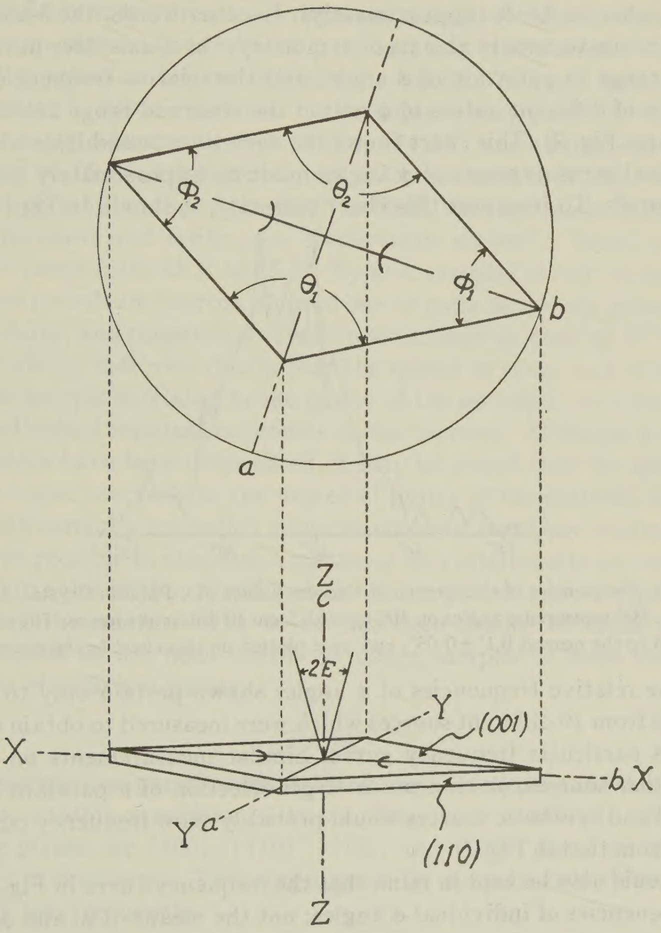

FIG. 1. Form and Optical Orientation of the Orthorhombic *n*-Paraffin Crystal.

In its simplest form, as illustrated, the crystal is a thin rhombic plate. In the figure, the thickness of the plate is exaggerated. It should be noted that since the angular measurements are made with the microscope and depend on the interior angles of the rhombic plate, all descriptive data are given in terms of these angles. The obtuse interior angle is designated as θ, and the acute interior angle as ϕ. Thus θ is equivalent to the conventional interfacial angle $(110)\wedge(1\bar{1}0)$, while ϕ is equivalent to $(110)\wedge(\bar{1}10)$.

The acute interior angles (ϕ in Fig. 1) are more variable within a single crystal than are the obtuse interior angles, θ. In crystals of very pure n-paraffins, $\phi_1 = \phi_2$ (approximately) and $\theta_1 = \theta_2$ (approximately). In mix crystals and in crystals of impure n-paraffin, as a general observation $\phi_1 \neq \phi_2$, whereas $\theta_1 = \theta_2$ (approximately). In other words, the b-axis of the crystal tends to remain an axis of symmetry; the a-axis does not.

The range in variation of ϕ angles and the relative frequencies of occurrence of different values of ϕ within the observed range are shown on the chart (Fig. 2). This chart shows the variations found from about 800 individual measurements of ϕ angles made on approximately 400 different crystals. To interpret this chart correctly, it should be kept in mind that the relative frequencies of ϕ angles shown pertain only to the 400 crystals from 10 different sources which were measured to obtain the data for this particular frequency curve. Similar measurements on crystals from other sources, or on a much larger selection of n-paraffins from all natural and synthetic sources would probably show frequency curves differing from that in Fig. 2.

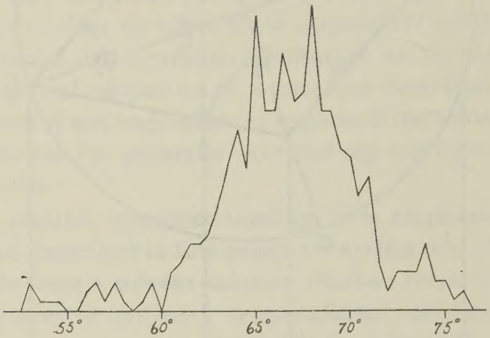

FIG. 2. Frequencies of Occurrence of Various Values of n-Paraffin Crystal Angles (ϕ). Data: 800 measured ϕ angles on 400 crystals from 10 different sources. The angles were measured to the nearest 0.1° ± 0.05°, and were plotted on this chart to the nearest 0.5°.

It should also be kept in mind that the frequency curve in Fig. 2 shows the frequencies of individual ϕ angles; not the means of ϕ_1 and ϕ_2 for the different crystals. In a single crystal the difference between ϕ_1 and ϕ_2 has been found to be as great as 20°, though the average difference is much less.

Several interesting features are evident from an inspection of Fig. 2. The frequency curve declines rapidly to 60° (the angle for a hexagonal crystal form), and remains low for all values less than 60°. Frequency peaks, in order of importance, are seen at 68°, 65°, 66.5°, 64°, 74°, and 71°. The peak at 74° represents very pure Octacosane ($C_{28}H_{58}$). The remainder of the data incorporated in the chart are from mix crystals of refined n-paraffins from petroleum sources.

In general, the entire range of ϕ values will not be found in mix crystals from any single source. Each sample of paraffin from a different source shows a characteristic frequency curve of ϕ angles, usually distinguishable in its form from ϕ-frequency curves of samples from other sources.

Numerous observations of both pure and mix crystals show that the range of ϕ values in a pure individual *n*-paraffin is quite limited, and much greater in the mix crystals. For example, a very pure *n*-Octacosane showed a sharp ϕ-frequency peak at about 74.25°, and a range of ϕ values from 73.5° to 75.5°. A sample of pure *n*-Dotriacontane ($C_{32}H_{66}$) showed a peak at 68° and a range from 65.5° to 69.5°. An equi-molar mixture of pure Octacosane and fairly pure Nonacosane showed a broad peak at 68° and a range from 63.5° to 75.5°. Typical samples of mix crystals, refined from petroleum sources, showed one or more frequency peaks, usually not sharp, and ranges in ϕ values in some cases as great as 15° or 20°.

The evidence indicates clearly that the spread or range in ϕ values for any given sample is related to the purity of the material, or to the number of individual *n*-paraffins present in the mixture. Although no exact relationships have been determined, it may be stated that the spread of ϕ values varies inversely as the degree of purity of the material crystallized. With carefully controlled molar mixtures of very pure *n*-paraffins it may prove possible to establish a mathematical relationship between the interfacial angles of the crystal and the molar percentages of *n*-paraffins comprising the mixture. The writer has been unable to make such a study because he has been unable to obtain samples of more than one *n*-paraffin of sufficient purity.

TWINS

The long chain *n*-paraffins crystallized from solution at ordinary temperatures, exhibit a variety of twins. The most commonly observed twinning planes are {100}, {110}, {310}, and {010}, listed in order of frequency of occurrence. Twinning apparently occurs in other directions, but much less frequently.

Micro-twinning is apparently responsible in many instances for curved {110} faces observed in *n*-paraffin crystals. In the majority of these instances, the curvature of the {110} faces is convex outward, but the reverse curvature is common in crystals of *n*-paraffin from certain sources.

Curved faces may also be produced where impurities are present in the solution, or in mix crystals containing several *n*-paraffins. Curvature is also common in crystals of the lower melting point members of the *n*-paraffin series when the temperature during crystallization is within 8° or 10°C. below the melting point.

It is sometimes difficult to determine whether the curved faces are the result of twinning, or of warping of the crystal structure produced by impurities, or of other factors. It has been observed that freshly formed perfect crystals may in the course of time develop curved or irregular faces. This is apparently the result of resorption produced by relatively low melting point amorphous wax or oil, which makes up the residual matrix surrounding the paraffin crystals after the solvent has evaporated. This feature is particularly noticeable where relatively low melting point crystals have not been stored in a cool place.

In addition to twinning, a common feature of *n*-paraffin crystals is the formation, by parallel growth on the {001} face, of one or more rhombic plates of successively smaller dimensions. These are usually more or less concentrically arranged, so that the entire crystal has the appearance of a very flat step pyramid.

Occasionally, and particularly in pure *n*-Octacosane, the successive steps or tiers of rhombic plates, instead of having a concentric arrangement, are superimposed in such a manner as to present the appearance of a spiral arrangement,[2] and in such cases, the pseudo-spirals may appear right-handed of left-handed, with no statistical evidence to indicate a tendency toward either direction.

BEHAVIOR IN PLANE POLARIZED LIGHT

In plane polarized light the pure crystals are colorless, translucent to transparent. They show no sign of pleochroism. When crystallized from solution on the microslide beneath a cover glass, the rhombic plates are so thin that a reduced or an oblique light is usually necessary to make them visible. The refractive indices of the crystals are commonly only slightly different from the index of the surrounding matrix. This matrix is composed of amorphous waxy materials, and shows few or no indications of crystalline structure.

In the case of extremely pure single members of the *n*-paraffin series, however, practically the entire area of the microslide preparation is crystalline. In such cases, it is unusual to observe euhedral crystals, formed free of interference from neighbors, and the true boundaries of crystals are difficult to observe without the use of crossed nicols.

BEHAVIOR BETWEEN CROSSED NICOLS

Between crossed nicols in parallel rays (without use of condenser lens) the crystals behave differently, depending upon whether the preparation is of a single very pure *n*-paraffin on the one hand, or on the other a mixture of two or more pure *n*-paraffins, or from one to several *n*-paraffins containing impurities. In general, pure preparations of a single *n*-paraffin compound show fairly marked double refraction in the *c*-axis direction, whereas the mix crystals and the impure preparations are usually feebly anisotropic, or practically isotropic (uniaxial).

---

[2] This form of parallel growth with a spiral pattern differs from the spiral structure in certain paraffin crystals described by Prof. Chas. M. Heck, North Carolina State College, Raleigh (Heck,1936).

Interference colors are invariably first order gray, even in the pure unmixed compounds. This is true for the thickest crystals that have been observed. The insertion of a gypsum plate effectively enhances the colors.

The following characteristics in parallel light between crossed nicols have been observed without exception in all *n*-paraffin crystals which are appreciably biaxial:

1. The faster ray vibrates approximately parallel to *b*.
2. Extinction is approximately symmetrical, but as will be described later, it is in some instances noticeably asymmetrical, and the extinction angle varies slightly with different crystals.
3. Double refraction characteristically varies within a single crystal where the thickness in the *c*-axis direction is variable. Many crystals are thicker in the center and thin out toward the margins, being roughly of the form of a flattened pyramid. In such crystals, the central portion may be rather strongly anisotropic, and the marginal zone apparently isotropic. This observation suggests that many crystals appear isotropic because of their very slight thickness.
4. When the *b*-axis of the rhombic plate is rotated into the "northwest" quadrant (with reference to the vibration planes of the nicols) the crystals show stronger double refraction than when the *b*-axis is rotated to the "northeast" quadrant. In thick, strongly anisotropic crystals, or in crystals of a single very pure *n*-paraffin, this phenomenon is not conspicuous, and might be missed if one were not looking for it. In the more feebly anisotropic crystals, and particularly in very thin crystals, this feature is striking. Such crystals, during a complete rotation of the microscope stage, may show double refraction only twice; both when the *b*-axis of the crystal is in the "northwest" quadrant. When the *b*-axis is in the "northeast" quadrant, there is either a very faint appearance of double refraction, or the crystal remains dark. There is nearly always complete extinction when the *b*-axis is parallel to the plane of the lower nicol. When the *b*-axis is parallel to the plane of the upper nicol, extinction is often incomplete. When the *b*-axis is oriented with the plane of the lower nicol, extinction is almost always symmetrical. When the *a*-axis is oriented with the plane of the lower nicol, however, extinction is often observed to be slightly asymmetrical. Wherever the angular positions of extinction and of maximum double refraction have been measured carefully, they have been found to be shifted or rotated slightly in a counter-clockwise direction from their normal positions (with the possible exception, previously noted, when the *b*-axis is parallel to plane of lower nicol).

In order to investigate more thoroughly the nature of this anomalous behavior, the microslides were in many cases placed up-side-down on the microscope stage, and the identical crystals observed again in the inverted position. The phenomenon remained unchanged, with maximum double refraction still in the "northwest" position, and the positions of extinction and of maximum double refraction shifted slightly counterclockwise.

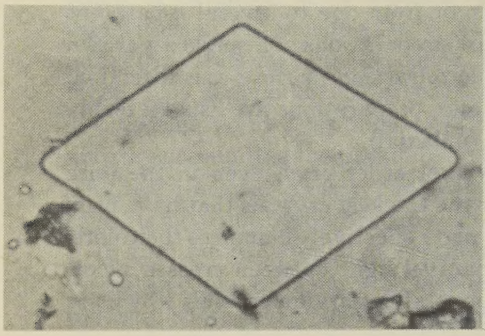

Fig. 3

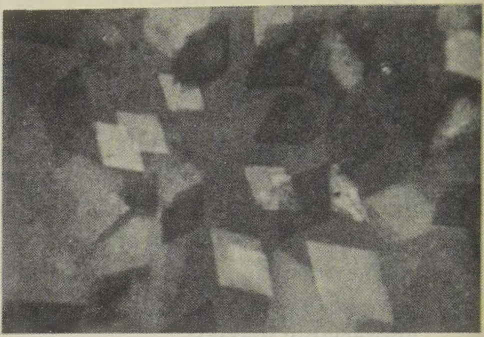

Fig. 4

Fig. 3. Photomicrograph in plane polarized light of a typical *n*-paraffin mix crystal of about 56°C. melting point, occurring in petroleum (Panhandle, Texas). Magnification ×415.

Fig. 4. Photomicrograph in polarized light of crystals of a pure synthetic *n*-paraffin (*n*-Dotriacontane, $C_{32}H_{66}$). Crossed nicols, with parallel light. Magnification 48×. Vibration planes of the nicols are parallel to edges of the photograph; P-P′ being "north-south" and A-A′ being "east-west."

The crystals seen in the photograph are all oriented with their *c*-axes "vertical" (normal to plane of the paper) and with their *b*-axes (long diagonal of the rhombic plate) oriented at random in the "horizontal" plane (plane of the paper). It will be observed that those crystals with *b*-axis aligned in the "northwest" quadrant show relatively strong double refraction, whereas those with *b*-axis parallel to vibration plane of either nicol or aligned in the "northeast" quadrant are dark, or show relatively weak double refraction. This anomalous behavior is explained as an effect of the optical rotatory power of the *n*-paraffins.

Behavior in Convergent Polarized Light

The interference figure is biaxial positive. Because of the invariable orientation of the crystals on the microslide with the *c*-axis in the vertical position, the interference figure always seen is the acute bisectrix figure. The isogyres show no accompanying isochromatic curves, due to the relatively small double refraction (β-α), and to the thinness of the crystals.

Mix or impure crystals show small optic angles, and in many cases the interference figure appears to be practically uniaxial. In pure unmixed *n*-paraffins, values of 2E have been observed as large as 41°. The usual range of 2E for distinctly biaxial crystals is between 20° and 40° Among the mix and impure crystals, the 2E angles range generally from 0° to 10° or 15°. Both in the strongly biaxial and in the approximately or apparently uniaxial crystals, the sign of the interference figure is invariably positive. No *n*-paraffins of opposite sign have been observed.

The writer has been unable to determine accurately the refractive indices of *n*-paraffin crystals in the three crystal directions. In the invariable orientation of the crystals on the microslide, only the β and α indices may be measured conveniently, and these two indices are usually nearly equal. Measurements of these have shown a range of values from 1.50 to 1.52. If the average of β for all the observed paraffins is assumed to be 1.51, then the observed range for distinctly biaxial crystals of $2E = 20°$ to 40° would correspond to the values $2V = 13°$ to 26°.

The interference figure is always central in the field of view, and shows no displacement when the microscope stage is rotated. Thus the acute bisectrix is parallel to the optical axis of the microscope, and normal to the (001) face of the crystal. No evidence of the slightest inclination of the acute bisectrix has been observed in any of the many *n*-paraffin crystals from all sources, both natural and synthetic. Because of the impossibility of thus detecting a slight inclination of the acute bisectrix, these observations do not necessarily prove that every crystal studied was either orthorhombic or hexagonal. The observations do, however, show that none of the strongly monoclinic crystal forms reported from *x*-ray studies, are to be found among the long chain *n*-paraffins crystallized from solution at temperatures well below transition and melting points.

As would be expected, in view of the previously described asymmetrical behavior of *n*-paraffin crystals between crossed nicols with parallel light, the behavior in convergent polarized light is also anomalous. Without any observed exception, even in the purest *n*-paraffins, the axial angle (2E) is definitely larger when the *b*-axis of the crystal is oriented in the "northwest" quadrant. This asymmetry is usually but not invariably more pronounced in those crystals showing 2E values somewhat below the average for all crystals studied. The degree of the asymmetry is fairly constant for all crystals from any one sample or source. This statement is particularly true of pure, unmixed *n*-paraffins.

Careful measurements of the axial angles of 24 crystals from 15 different sources, ranging from very pure *n*-paraffins to mixtures and impure preparations, and including both natural and synthetic *n*-paraffins, showed the following results:

2E(N.W.)—Range 17.8° to 41.6°; arithmetic mean = 30.2°.
2E(N.E.) —Range 15.3° to 38.9°; arithmetic mean = 25.0°.
2E(N.W. and N.E.)............. arithmetic mean = 27.6°.

Maximum asymmetry measured in a mix crystal; 2E(N.W.) = 30.9°; 2E(N.E.) = 20.4°.
Minimum asymmetry measured in a pure crystal; 2E(N.W.) = 40.7°; 2E(N.E.) = 38.9°.
Minimum asymmetry measured in a mix crystal; 2E(N.W.) = 22.1°; 2E(N.E.) = 20.4°.

All determinations of 2E on individual crystals represent means of repeated measurements. The probable errors of the means are in most cases less than ±0.5°.

Interpretation of Anomalous Behavior in Polarized Light

The previously described anomalous behavior of *n*-paraffin crystals between crossed nicols shows that these crystals are optically active. The observations furthermore show that all the crystals thus far examined are dextrorotatory.

The dextrorotatory action of the *n*-paraffin crystal is illustrated graphically in Fig. 5. The left diagram (Fig. 5*a*) represents a crystal with the *b*-axis oriented at 45° in the "northwest" quadrant; the right diagram (Fig. 5*b*) another crystal with the *b*-axis oriented at 45° in the "northeast" quadrant. In both diagrams lines PP′ and AA′ represent the vibration directions of the lower and upper nicols respectively. In each diagram the *b*-axis of the crystal is shown by a solid line; the *a*-axis by a dashed line (cf. Fig. 1). The projection of the vertical *c*-axis on each diagram at the intersection of the *a* and *b* axes, and is designated by the letter *C*. The *c*-axis of the crystal on each diagram coincides with the optical axis of the microscope. The distances CB = CB′ represent the amplitude of the plane polarized ray emerging from the lower nicol.

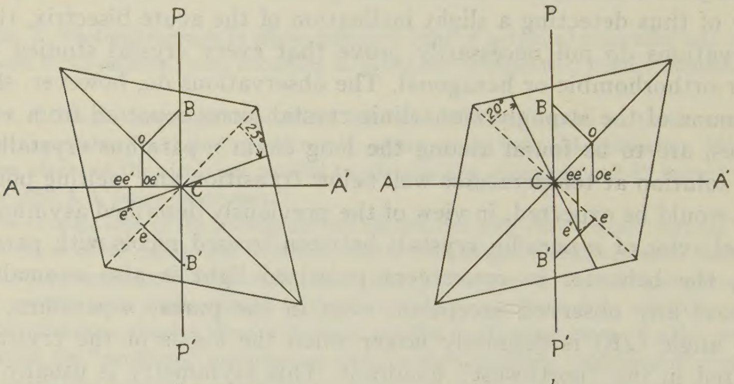

a *b*

Fig. 5. Optical Rotation of *n*-Paraffin Crystal Between Crossed Nicols.

When this polarized ray enters the crystal, it is split into two polarized rays, the ordinary, or (*o*) ray and the extraordinary, or (*e*) ray. If the *n*-paraffin crystal were optically inactive, the (*o*) ray would vibrate through the crystal in a direction parallel to the *b*-axis, and the (*e*) ray would vibrate parallel to the *a*-axis.

An optically active dextrorotatory crystal would produce a clockwise rotation of the vibration direction of one or of both rays. Observations of *n*-paraffin crystals indicate that the amount of rotation suffered by the (*o*) ray is usually small or negligible. For greater simplicity, therefore, the (*o*) ray in Figs. 5*a* and 5*b* is assumed to have undergone no rotation. The clockwise rotation of the (*e*) ray is shown by a solid line in both diagrams. The amount of rotation is about 25° in Fig. 5*a* and about 20° in Fig. 5*b*.

At the 45° position the component amplitude of the (*o*) ray which emerges from the crystal is represented by the distance C–o, found by dropping a perpendicular from B to the *b*-axis. A perpendicular to AA′ is then dropped from the point (o) to point (oe′) on AA′. Then the distance C–oe′ represents the component amplitude of the (*o*) ray which emerges from the upper nicol.

The (*e*) ray, which like the (*o*) ray, originates the instant the plane polarized light enters the crystal from below, vibrates initially parallel to the *a*-axis (dashed lines in Figs. 5*a* and 5*b*). The component amplitude of the (*e*) ray while passing through the crystal is represented by the distance C–e, found by dropping a perpendicular to the *a*-axis from the point B′. In passing through the crystal the plane of vibration of the (*e*) ray is rotated in a clockwise direction, so that on emerging from the upper surface of the crystal the ray has changed its vibration direction from C–e to C–e′. A perpendicular to AA′ dropped from (e′) to (ee′) gives the distance C–ee′, which is the component amplitude of the rotated (*e*) ray which emerges from the upper nicol. The sum of the components C–oe′ and C–ee′ gives the total amplitude of the combined rays emerging from the upper nicol.

It may be visualized from Figs. 5*a* and 5*b* that as the dextrorotatory crystal is rotated on the microscope stage between crossed nicols, the sum of the components of the two emergent rays (oe′ and ee′) will vary greatly, and the pattern of the variation will differ from that of an optically inactive crystal. The pattern will also depend on the amount and direction of rotation of either or both rays emerging from the crystal.

To illustrate the effect of optical activity, the two curves in Fig. 6 show the changes in relative intensity of transmitted light as the crystal is rotated (between crossed nicols) through 180° in a clockwise direction, starting (on the left) with the *b*-axis parallel to the vibration plane of the upper nicol. The dashed line curve is that of an optically inactive crystal. The solid line curve is that of a *n*-paraffin crystal in which the (*o*) ray has undergone no rotation, and the (*e*) ray has undergone a clockwise rotation of 20°. The curves need not be extended as they are repeated over each 180° rotation of the crystal.

The solid line curve (for an optically active crystal) in Fig. 6 illustrates qualitatively several observations of the anomalous behavior of *n*-paraffins in parallel polarized light which have been described previously.

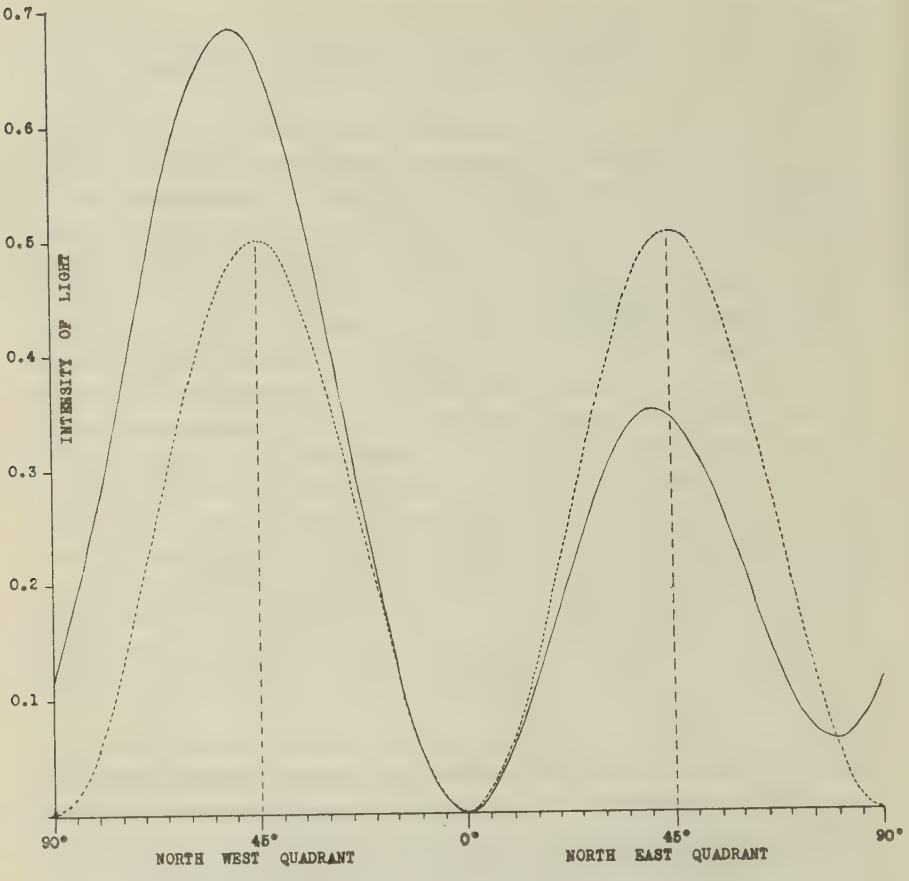

FIG. 6. Orientation of *b*-Axis of Crystal vs. Light Intensity.
Dashed Line Curve; r = 0°
Solid Line Curve; r(o) = 0°
r(e) = +20°

These are:

1. Light intensity is invariably greater with the *b*-axis at 45° in the "northwest" quadrant than at 45° in the "northeast" quadrant.
2. Extinction is often incomplete and slightly asymmetrical with the *b*-axis in the "east-west" position.
3. Extinction is usually complete and symmetrical when the *b*-axis is in the "north-south" position.
4. Positions of maximum light intensity and positions of extinction (where measurably asymmetrical) are always shifted counter-clockwise from their respective normal positions.
5. In the case of a thin crystal, or one with weak double refraction, the light intensity maximum in the "northeast" quadrant would not be observed, and the crystal would appear to remain dark through 180° of rotation on the microscope stage.

The solid line curve in Fig. 6 is intended to illustrate only qualitatively what actually happens. It is not intended to imply that only the extraordinary ray is rotated; and it may be assumed that both the (*e*) and (*o*) rays undergo amounts of rotation which vary with the structure and thickness of each individual crystal. However, observations suggest that the (*e*) ray is rotated more than is the (*o*) ray in the great majority of *n*-paraffin crystals.

In order to check further the theoretical asymmetry shown in Fig. 6 against actual behavior of the *n*-paraffin crystal in polarized light, a single crystal was selected, and a number of repeated measurements made and averaged. The crystal selected was a fairly large distinctly biaxial mix crystal, the melting point of which was later found to be about 61° C. The axial angles (2E) were 27.4° (N.W.) and 24.8 (N.E.). The results of the measurements are recorded in Table 1.

TABLE 1

Obs. No.	Light filter used	Approx. wave length of incident light-peaked at:	λ (N.W.)	λ (N.E.)	Sum	No. of repeated measurements	Probable error of mean
1(a)	Red shade yellow Corning No. 3480	Above 610 mμ	48.0°			10	±0.6°
1(b)	Red shade yellow Corning No. 3480	Above 610 mμ		36.2°	84.2°	10	±0.6°
2(a)	None	Approx. 589 mμ	48.4°			10	±0.5°
2(b)	None	Approx. 589 mμ		43.8°	92.2°	10	±0.3°
3(a)	Dark blue green Corning No. 4303	Below 520 mμ	48.3°			10	±0.7°
3(b)	Dark blue green Corning No. 4303	Below 520 mμ		45.0°	93.3°	10	±0.4°

Light source was 10 watt tungsten lamp with Corning "Daylight" glass.

In this table, the angle λ is the angle between the plane of the lower nicol and the *b*-axis of the crystal when the crystal is rotated to the position of maximum light intensity in the quadrant indicated.

The results shown in Table 1 agree qualitatively with the theoretical requirements illustrated in Fig. 6. Thus it is evident that in dextrorotatory crystals the peaks of light intensity are displaced in a counter-clockwise direction. Still another feature brought out in Table 1 is the indication that the longer the wave length of the transmitted light, the greater the counter-clockwise shift of the light intensity maximum in the "northeast" quadrant.

It is obvious from the preceding observations that it would be possible to determine with fair accuracy the amount of optical rotation in a *n*-paraffin crystal by measuring accurately, with monochromatic light, the positions of extinction and of light intensity maxima, and the relative peak intensities. To determine the specific rotation, the thickness of the crystal would have to be measured. Thus it would be possible, and of interest, to compare the specific optical rotation of a paraffinic petroleum or petroleum fraction with the calculated specific rotation of *n*-paraffin crystals extracted from the same petroleum.

CAUSE OF OPTICAL ACTIVITY OF *N*-PARAFFIN

It has been pointed out that whereas the observed optical asymmetry of the *n*-paraffin crystal between crossed nicols is often quite pronounced in the impure and mix crystals, it is still clearly present in the purest synthetic *n*-paraffin crystals. It is therefore highly probable that this optical activity is caused by the internal structure of *n*-paraffin, and not necessarily by the presence as impurities of some foreign organic compounds, as seems generally to have been assumed in the case of paraffinic petroleums.

In the above connection, Gruse and Stevens (1942) state: "Optical rotatory power is exhibited by nearly all crude oils. The majority of them are dextro-rotatory; some are laevo-rotatory; and only a few appear to be inactive. The optical activity is not uniformly distributed throughout the distillation range of the crude but is usually a maximum for the intermediate fractions. Curiously, the maximum occurs at about the same boiling point for all crude types, 250° to 300° C. at 12 mm. Hg., but no extensive data have been collected on this point. No activity has been observed in fractions boiling below 200° C. at atmospheric pressure. The decrease in activity above the maximum may be partly due to racemization by heat. The existence of optical rotation of oils has given much weight to the organic theories of the origin of petroleum."

Of course a considerable number of organic compounds, known or believed to be present in petroleum, could cause the observed optical activity. It is perhaps significant, however, that the range of crude oil fractions showing the maximum optical activity corresponds in a general way with the range of fractions which in paraffinic crudes contain most of the long chain *n*-paraffin waxes. The fact that the majority of crude oils are dextrorotatory is likewise significant. Absence of optical activity in a crude oil might be due to racemization, or it might be due to absence of optically active constituents, such as long chain *n*-paraffins. The laevorotatory activity of some crude oils may be caused by the presence of laevorotatory hydrocarbons. At least, the evidence presented in the present paper would seem to show that the laevorotatory activity, exhibited by some crude oils, cannot be due to the presence of *n*-paraffins.

It has been shown by Müller (1928, 1929) that the molecules of the long chain *n*-paraffins are arranged with their long axes parallel to the *c*-axis of the crystal, and the ends of the molecules lie in planes normal to the *c*-axis. Müller (*ibid.*) and others (Piper *et al.*, 1931; Kolvoort, 1938; Gray, 1943) have also shown that under certain conditions at least some members of the *n*-paraffin series may have the long axes of the molecules inclined to the *c*-axis and to the {001} planes.

In the present paper it has been shown that when *n*-paraffin crystals form from solvent solutions at ordinary temperatures well below transition and melting points, the molecular chains must be vertical, or parallel to the *c*-axis of the crystal, and that the crystals are primarily orthorhombic. Under the conditions specified, no definitely monoclinic crystals have been observed.

It appears that nothing in the packing arrangement or attitude of the *n*-paraffin chains in forming the crystal unit cells and the lattice can explain the observed optical activity. If the optical activity is not caused by the presence of foreign material in the inter-molecular spaces of the lattice, then it can only be produced by the internal structure of the *n*-paraffin molecule.

Müller (1928) working with one or two perfect crystals of very pure *n*-Nonacosane, carried out the only complete *x*-ray study that has been made of any long chain *n*-paraffin. This work has become classical, and Müller's conclusions on the structure of the long chain *n*-paraffin molecule and crystal lattice have become generally accepted.

Briefly stated, Müller found the *n*-paraffin molecular chain to be a zig-zag form, in which the carbon atom centers all lie in one plane, and in that plane, form two vertical rows on opposite sides of, and equidistant from the zig-zag chain axis. Instead of the carbon-carbon bonds forming, one with the next, the tetrahedral angle of 109° 28′, as might be expected from the known tetrahedral form of the carbon atomic domain, the zig-zag angle was found to be between 76° and 92°. The chain axis was found to be parallel to the *c*-axis of the crystal, and the zig-zag planes of the molecules were found to lie at an angle to the *b*-axis of the crystal of somewhere between 23° and 30°. In any single {001} layer of molecules, half the molecules have their zig-zag planes rotated 23°–30° clockwise; the other half counter-clockwise. In each {001} layer of molecules, the molecules are staggered along rows which are parallel to the *a*-axis. Each row alternately has molecules with zig-zag planes rotated clockwise or with planes all rotated counter-clockwise.

The above described zig-zag molecule and crystal lattice (for orthorhombic crystal forms) have come to be generally accepted as representing the true structure of the long chain *n*-paraffin series. There is nothing in this molecular structure or in this lattice structure which can explain the observed dextrorotatory optical activity of *n*-paraffins, and it is therefore apparent that in some respects, Müller's reconstruction from *x*-ray data must be in error. In general, the results of the optical studies described in the present paper do not disagree with Müller's reconstruction of the crystal lattice. Exception is taken only to Müller's reconstruction of the molecule, on the grounds that the optical observations tend to confirm the essential accuracy of Müller's reconstruction of the crystal lattice, and that neither this lattice arrangement nor the zig-zag form molecule can account for the observed optical rotation.

Spiral Structure of the Long Chain *N*-Paraffin Molecule

As a working theory, subject to confirmation by further investigations, it is suggested that the long chain *n*-paraffin molecule has a spiral structure.

Starting with this basic assumption, which is not new as applied to some other long chain compounds, certain other reasonable assumptions will be made. These are:

1. The diameter of the carbon atom domain, or length of the C-C bond, is 1.54 Å, as in diamond.
2. Adjacent C-C bonds form the tetrahedral angle, 109° 28′. From this assumption, a spiral or solenoidal arrangement of carbon centers is a logical consequence.
3. Of many different geometrically possible tetrahedral spirals, the two simplest arrangements are selected, and from these two, the left handed spiral is chosen. (See photo of model, Fig. 7.)
4. The C-H bonds also form the tetrahedral angle with all other bonds from a common center. This assumption may be unnecessary to explain the optical rotation. It is made merely to complete the picture in an orderly manner.

From the foregoing assumptions, the following relationships and dimensions of the spiral chain (see Fig. 7) have been calculated:

1. The carbon atom centers are spirally arranged around the chain axis, being equally spaced on a left-handed helix, the parametric equations of which are; $x = R \cos \theta$; $y = R \sin \theta$; $z = K\theta$, where $R = 0.534$ Å, $K = 0.5189$, and $\theta = 131° \, 43.94'$ ($= 2.2991629$ radians).

2. Various dimensions and angles are:
   - (a) Diameter of the helix = 1.068 Å.
   - (b) Cross sectional area of helix = 0.895 $(Å)^2$.
   - (c) Inclination of C-C bonds to direction of chain axis = 39° 14.035′.
   - (d) Spacing (in direction of chain axis) of successive carbon centers = 1.193 Å.

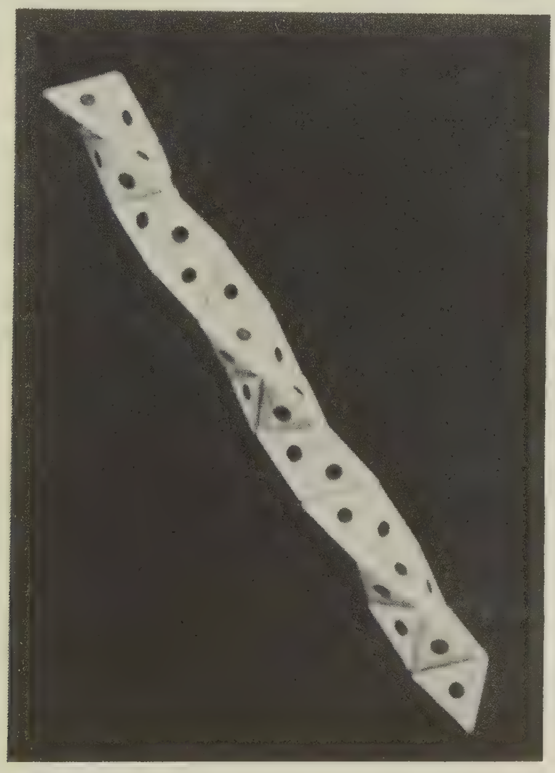

FIG. 7. Model of a spiral molecule of *n*-paraffin (*n*-Octacosane). The centers of the tetrahedrons correspond with the carbon atom centers, which fall on a helical curve. For greater convenience in constructing the model, the carbon-carbon bonds are made to intersect the tetrahedron face centers rather than the corners. The helical arrangement of the carbon atom centers is the same in either arrangement. Positions of the hydrogen atoms are shown by the black dots.

3. The molecule has no plane of symmetry.
4. As is evident from the calculated value of θ, no two carbon centers in a chain of any reasonable finite length lie in vertical alignment. There is, however, an approximate repetition or cycle for every eleventh carbon atom. Thus, C-12 is situated almost vertically below C-1; C-13 below C-2; C-14 below C-3, etc.

A reconstruction of the assumed *n*-paraffin spiral molecule is shown in Fig. 7, which represents a chain of 28 carbon atoms (*n*-Octacosane). For convenience in construction, the C–C bonds are made to intersect the tetrahedron face centers, though they could as well be drawn through the tetrahedron corners. The result is the same as long as the bond length of 1.54 Å is retained. The hydrogen atoms are represented on the model by black dots at the centers of the "free" tetrahedron faces. It is seen that in addition to the spiral arrangement of the carbon centers, there are six spirals made by the hydrogen atoms in the CH_2 groups It is not necessary to assume that the hydrogen spirals exert any influence in producing the observed optical activity.

TABLE 2

Measurement	Müller	Spiral Theory	Remarks
Length of C-C Bond	1.8 to 2.0 Å	1.54 Å (exactly)	
Distance between 2 vertical rows	1.2 to 1.6 Å	No rows exist	Diam. of helix = 1.068 Å
Dist. between consecutive centers in either row	2.537 Å ±0.5%	No rows exist	Dist. parallel to chain axis between alternate carbon centers = 2.386 Å
Zig-zag angle	76° to 92°	Tetrahedral angle = 109° 28′	If C–C bonds were projected on plane parallel to chain axis, apparent angle would vary between 109° 28′ and 180°.
Angle between C–C bonds and chain axis direction	44° to 52°	39° 14.035′	Projected on plane as per above, apparent angle would vary between 0° and 39° 14.035′
Angle between zig-zag plane and crystal *b*-axis	23° to 30°	non-existent	

For comparison, Table 2 shows the spacings and angular relationships of the carbon centers as reconstructed by Müller from *x*-ray studies, and as result from the spiral arrangement described above.

According to Müller's calculation of 2.537 Å for the distance between carbon centers along either row of the zig-zag chain, the addition of one carbon atom would increase the chain length by 1.2685 Å ± 0.5%. With a spiral chain of the dimensions described, the corresponding increase in chain length would be 1.193 Å. It should be noted, however, that Müller's value corresponds to a calculated C–C bond length of about 1.9 Å whereas we have assumed for our spiral chain a bond length of 1.54 Å. If we were to assume a bond length of 1.9 Å for the spiral chain, the addition of one carbon atom would increase the chain length by 1.47 Å.

Whether or not Müller's *x*-ray data could be re-interpreted to fit a spiral molecule is a question beyond the scope of the present paper. It is, of course, possible that the zig-zag type of chain exists in some *n*-paraffins, or in all *n*-paraffins under some conditions. On the other hand, the optical evidence presented appears definitely to favor the spiral form, as it is difficult to visualize how either the zig-zag chain or the lattice structure could produce the observed optical rotation. Several thousand individual *n*-paraffin crystals from many sources have been studied in polarized light. Among these not a single crystal was observed which failed to show the characteristic indications of optical activity.

BEHAVIOR OF *N*-PARAFFIN CRYSTALS ON HEATING

REVIEW OF PREVIOUS WORK AND THEORETICAL CONSIDERATIONS

Members of the *n*-paraffin series, when isolated in a very pure state, may be identified by the melting points, as is well known. The melting points for the series have been shown to lie on a smooth curve. In the case of mixed *n*-paraffins, Piper and co-workers (1931) showed that the purity of a paraffin sample, or the identities of the two or more paraffins in a mixture, cannot be determined from the melting point alone. However, the same investigators showed from experiments with *n*-paraffins of known purity, and with known mixtures of these, that the purity of a sample and considerable information about the identities of components in an unknown mixture of *n*-paraffins can be determined by observing the difference between the transition temperature (on heating) and the melting point. It was also established by these same authors that there is an alternation in transition points (on heating), the differences between the corresponding transition and melting points being from 1°C. to 2°C. greater for *n*-paraffins with odd-numbered chains than for even-numbered. This alternation was observed through the *n*-paraffin series within the range from C_{26} to C_{34}.

This alternation in the physical properties of the odd- and even-numbered *n*-paraffins was cited by Müller as confirmatory evidence supporting his thesis of the zig-zag form of the molecule. From purely geometrical considerations, it would appear that a zig-zag molecular chain would be more in accord with the observed alternation in physical properties than would a spiral chain. It seems possible, however, that this alternation of properties may be explainable on a chemical basis rather than geometrical.

It is generally agreed that the transition point (on heating) marks the rupture of the inter-chain terminal bonds between adjacent end-to-end molecules. According to Müller, this means that the chains retain their fixed relative positions in the crystal lattice, but are freed to rotate around their axes. It seems more likely that on reaching the transition temperature, the chains are not only freed to rotate on their axes, but also freed to move laterally in any direction normal to the *c*-axis, and thus to rearrange themselves from an orthorhombic packing into a hexagonal packing. When the temperature is raised to, and beyond the transition point, it is probable that the crystal would change from an orthorhombic to a hexagonal form, and the original ϕ angles of the crystal would change abruptly, decreasing toward the 60° angle as the melting point is approached. Observations supporting this interpretation will be described later.

The *n*-paraffin molecule has generally been regarded as built up of a series of CH_2 groups, capped at each end by a CH_3 group. On this basis, there should be no alternation of physical properties of odd- and even-numbered members, except for the geometrical difference pointed out by Müller. In a zig-zag chain which is even-numbered the C–C bonds at the ends of the chain are parallel; in the odd-numbered chain they are not.

However, the writer has noted other apparently constant differences between odd- and even-numbered *n*-paraffins, which are not as readily explainable by the geometrical difference between the odd- and even-numbered molecule. Crystals of even-numbered *n*-paraffins have larger average ϕ angles than do crystals made up wholly or largely of odd-numbered members of the *n*-paraffin series. The even-numbered crystals also tend to be more strongly orthorhombic in their symmetry, and to have larger axial angles. These observations are only of qualitative value, and will be checked quantitatively when a sufficient number of pure *n*-paraffins can be obtained for study. Nevertheless, differences in form, structure, and crystallization habits do exist between odd- and even-numbered crystals, and these differences are more easily visualized as differences in the lattice dimensions than as differences of geometrical form of the molecules.

It is suggested that the alternation of transition points on heating, as well as the above described differences in crystal form, which serve to distinguish the odd from the even members of the *n*-paraffin series, are caused by chemical differences in the two types of molecule. If we regard the "building blocks" of the *n*-paraffin chain as C_2H_4 and C_4H_8 groups, rather than as the conventional CH_2 groups, then we have the basis for assuming a difference in chemical properties between the odd and even molecule.

The evidence supporting this suggestion is indirect. Chibnall and Piper (1934) have shown rather conclusively that all long chain *n*-fatty acids and primary alcohols found in nature (various plant and insect waxes) have even-numbered chains, whereas all *n*-paraffin waxes from these natural sources have odd-numbered chains. These authors showed how the metabolic processes within plants might decarboxylate a fatty acid to form a corresponding *n*-paraffin with one less carbon atom.

It is difficult to explain the synthesis by plants of even-numbered acids and alcohols exclusively unless the plants are assumed to utilize as "building blocks" short straight chain molecules of even number carbon atoms. If we assume that in the plant metabolism long chain odd-numbered *n*-paraffin are synthesized, and some of them later carboxylated to form even-numbered acids, we are faced with the difficulty of explaining why both odd- and even-numbered paraffins are not found among the plant waxes.

The assumption of primitive "building blocks" with even numbers of carbon atoms, perhaps synthesized during early metabolic processes in plants, would appear to explain the observations of Chibnall and Piper. It is suggested here that these primitive "building blocks" probably included both C_2H_4 and C_4H_8 groups. If only the latter group existed, then it would be difficult to explain why the fatty acids and primary alcohols with 26, 30, and 34 carbon atoms are about as abundant among the plant waxes as are those with 24, 28, and 32 carbon atoms. On the other hand, the C_4H_8 group is the shortest chain which can define a right or a left handed spiral. It has been shown in the present paper that all the *n*-paraffins are dextrorotatory. If we assume that the primitive "building blocks" were C_2H_4 groups exclusively, then it is necessary also to assume an inherent tendency in these groups to join in a left handed spiral.

If the long chain molecules were all synthesized from original short chain groups, such as C_2H_4, having an even number of carbon atoms, then an odd-numbered *n*-paraffin may be regarded as having at one end an incomplete or ruptured "building block" (such as a CH_3 group), and at the other end a normal C_2H_5 (or C_4H_9) group. In a crystal lattice of an even-numbered *n*-paraffin, the inter-molecular bonds of end-to-end molecules would all be between like groups. In a lattice of odd-numbered chains, the end bonds would either all be between unlike groups, or between CH_3 groups in one {001} interface, and between C_2H_5 groups in the next interface, thus alternating throughout the crystal lattice. The latter arrangement would be in agreement with Müller's *x*-ray findings that the *c*-spacing in odd-numbered *n*-paraffins is equivalent to the length of two molecules, and only equivalent to the length of one molecule in the even-numbered paraffins. The arrangement would also account for the observed alternation of transition points on heating, provided we assume that the CH_3–CH_3 bond is less stable than the C_2H_5–C_2H_5 bond.

CHANGES IN CRYSTAL FORM ON HEATING

Müller (1930, 1932) measured the lattice dimensions of fifteen *n*-paraffins ranging from C_{18} to C_{44} at different temperatures by means of a series of *x*-ray photographs. He showed that the dimensions of the (*a*) and (*b*) axes of the unit cell changed with change of temperature. His results may be summarized as follows:

1. On heating, the series C_{21} to C_{29} changed from lower symmetry to hexagonal symmetry, the latter being reached just below the melting point.
2. On heating, the series C_{18} to C_{20}, and those above C_{29} tended to approach hexagonal symmetry, but melted before arriving at hexagonal symmetry.
3. C_{21} and C_{23} showed continuous change in (*a*) and (*b*) unit cell dimensions with increasing temperature up to the melting point. The *n*-paraffins C_{24}, C_{25}, C_{26}, C_{27}, C_{29}, C_{30}, C_{31}, C_{34}, and C_{44} showed abrupt transitions between room temperatures and their respective melting points.

The unit cell dimensions of the *n*-paraffins at different temperatures as determined by Müller may be used to compute the corresponding interfacial angles ϕ of the crystals. Some of Müller's results, thus converted to ϕ angles, are shown on the chart, Fig. 8. Also on the same chart is a curve for the ϕ angles of pure Octacosane (C_{28}) for different temperatures. This curve is based on direct measurements of the crystal on the microscope heating stage, and represents the mean of two series of observations on two different microslides. The two original observed curves, however, are practically identical with the mean shown in Fig. 8. The errors of the observed points on the original curves were estimated to be less than ±0.1° for the ϕ measurements, and approximately ±0.2°C. for corresponding temperatures.

In the first experiment, the crystal temperature was raised from 24.5°C. to 58.5°C. over a period of 3.5 hours at the nearly constant rate of 0.16°C. per minute. In the second experiment, the crystal temperature was raised from 23.5°C. to 56.9°C. over 2.25 hours at the average rate of 0.25°C. per minute.

Both original curves showed two definite transition points with rising temperature. The first (or lower) transition point was at 39.3°C. in each experiment. The second (or upper) and principal transition point was at 57.3°C. in the first experiment, and at 56.6°C. in the second experiment.

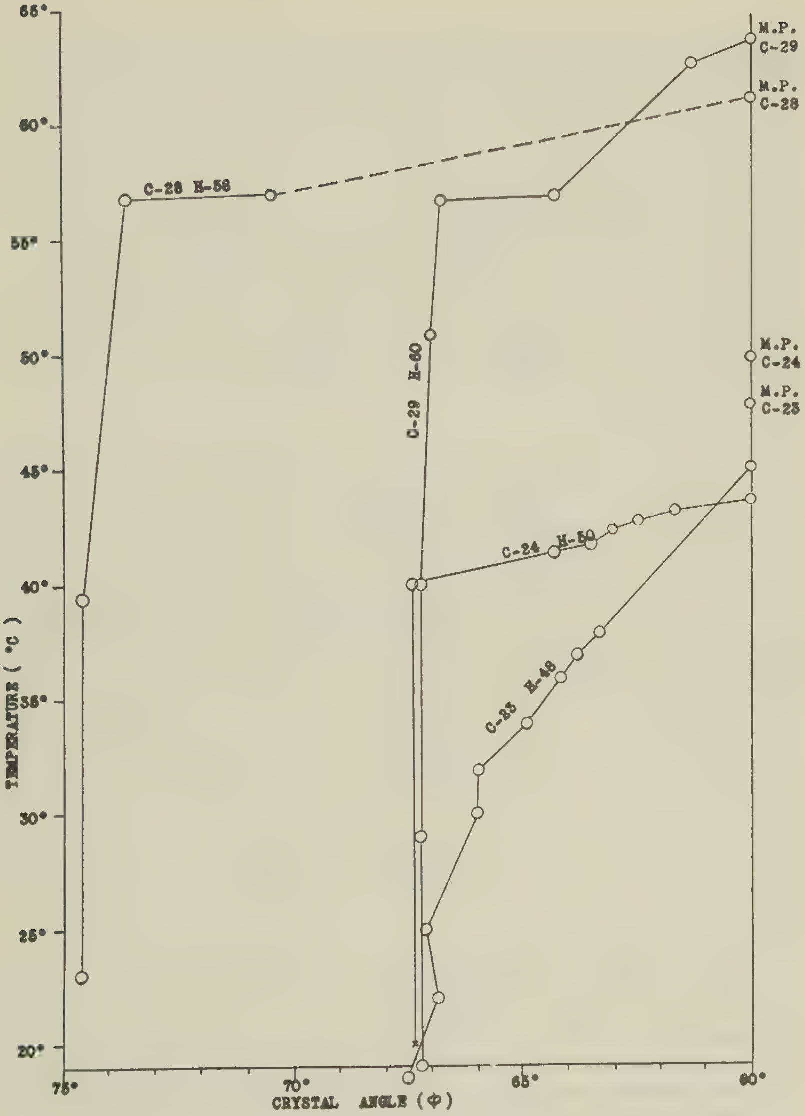

Fig. 8

The mean value, 56.9°C., is shown in Fig. 8. It will be observed that up to the temperature of 39.3°C., no change whatever took place in the crystal angles. From 39.3°C. to about 56.9°C. there was a linear decrease of about 1° in the ϕ angles. At 56.9°C. there was a very sudden decrease of about 3° in the ϕ angles. It will be noted in Fig. 8 that this ϕ-temperature curve for C_{28}, based on direct measurements of the changing crystal angles, shows a close parallelism to the curve for C_{29}, computed from Müller's x-ray measurements of the unit cell.

In the two experiments on C_{28} crystals, the temperature increase was carried to about 58°C. (3.5°C. below the melting point) and then allowed to decrease at uniform rates to room temperature over periods of two hours and four hours respectively. In each experiment the crystal {110} faces became somewhat irregular or warped at temperatures immediately above 56.9°C. (the upper transition, heating). During cooling below that point, still other irregularities appeared in the crystals, all of which had been completed on cooling to about 50°C. There were no further changes apparent in the crystals on cooling from 50°C. to room temperature.

The changes during cooling were observed between crossed nicols, with gypsum plate. It was evident that the setting of the crystals was accompanied by an irregular reorientation of the lattice structure, and that the changes described were not merely surface or resorption phenomena. After cooling to room temperature, the measured crystals, as well as others on the same microslides, were studied conoscopically. The interference figures were for the most part diffuse, due evidently to the irregularities in the lattice structure. The most significant observation noted, however, was that the dextrorotatory optical activity was still present, though in many instances, the positions of extinction and of maximum double refraction had been shifted varying amounts with respect to the original axes of symmetry of the crystals.

INTERPRETATION OF HEATING STAGE OBSERVATIONS

The interpretations of the foregoing observations are summarized as follows:

1. The first transition on heating (39.3°C. in C_{28} and about 40°C. in C_{29}, from Müller's data) marks a sudden "weakening" of the intermolecular end-bonds, permitting a progressive distortion of the orthorhombic lattice in the direction of hexagonal packing.
2. The second transition (This corresponds to Piper's "First Transition"—see Piper, 1931) represents sudden rupture of the end-bonds of most of the molecules, and the initiation of a "mass movement" of the molecules toward hexagonal packing, as the ϕ angles of the crystal decrease rapidly toward the limiting value of 60°. If it were possible to bring all portions of the lattice to the transition temperature at exactly the same instant, the ideal curve would presumably be "flat" at this temperature. In other words, the ϕ angles would decrease instantly to 60° when the crystal reached the transition temperature. It is also possible that the 60° ϕ angle could be reached by maintaining the crystal at exactly the transition temperature for a sufficient time to allow the molecules to move into the hexagonal pattern.

3. By allowing the crystal to cool before it had reached the melting point and before the entire lattice had reached the hexagonal form, a distorted lattice resulted, consisting of various segments, some orthorhombic, others more nearly hexagonal. This heterogeneity of the lattice is responsible for the observed warped and irregular crystal faces.
4. The fact that the dextrorotatory behavior of the crystals persisted after the crystals had cooled from temperatures above the upper transition point, and in spite of the disarrangements in the lattice structure, confirms the interpretation that the optical activity of *n*-paraffin crystals is produced by the internal structure of the molecule, and not by any peculiar orientation or arrangement of the molecules in the lattice.
5. It will be noticed that Müller's curve for C_{23} (shown in Fig. 8) differs radically from the curves for C_{24}, C_{28}, and C_{29}. As mentioned above, Müller found that C_{21} also behaved in the same manner as C_{23}. Incomplete heating stage observations of mix *n* paraffin crystals indicate behavior somewhat similar to C_{21} and C_{23}, which suggests that the samples of C_{21} and C_{23} used by Müller may not have been pure compounds.

GROWTH OF *N*-PARAFFIN CRYSTALS FROM SOLUTION

One of the most interesting aspects of the study of normal paraffin crystals, is to be found in observing through the microscope their growth, either from solution at ordinary temperatures, or from the melt. The present paper, however, is concerned only with the crystals formed from solvent solution at temperatures well below melting and transition points. Under such conditions, many observations were carried out with different optical combinations, including plane polarized light, crossed nicols with parallel light (with and without gypsum plate), and conoscopic observations of the interference figure.

A complete summary of these observations would be unnecessarily lengthy, and for present purposes it is sufficient to record only the following observed features, which are believed to have a bearing on the form of the crystal lattice, and the manner in which it is built up from a solvent solution of the paraffin.

1. In oblique or reduced ordinary or plane polarized light, the crystals make their first appearance out of solution as full sized crystals; that is, the rhombic plate has attained its maximum dimensions in the plane of the *a* and *b* axes. The first appearance of the crystal is sudden, because at this stage of growth the crystal is a very thin rhombic plate, and is at the lower limit of visibility. The "suddenness" of appearance is therefore an optical illusion. During the course of minutes, the outline of the crystal becomes progressively clearer. The refractive indices of the crystal are in almost all cases higher than that of the surrounding liquid or amorphous medium.
2. The same phenomena may be observed between crossed nicols, with and without a gypsum plate. With the gypsum plate, the interference colors, ranging between blue and yellow, are seen to increase gradually in intensities, the colors changing with the increase in thickness of each crystal.
3. Conoscopically, the changes observed are similar. The interference figure, during early stages of crystal growth, is invisible, then very faint, and gradually strengthening to normal visibility. During this change, the axial angle remains constant.

4. In the case of twinned crystals, the twins make their appearance simultaneously and in the same manner as described for the single crystal.

The most probable interpretation of the phenomena described above is that the initial stage of the crystal growth is the attachment of molecules to the glass surface (both microslide and cover glass) as a single layer of molecules. The molecular chain axes are normal to the glass surface. The molecules arrange themselves in the orthorhombic packing found in the finished lattice. This primitive layer grows laterally until it attains the full (*a*) and (*b*) dimensions of the completed crystal.

The second and subsequent stages of crystal growth consist in the consecutive additions of identical layers on the primitive layer, the process continuing until stopped by (a) interference of opposite glass surface, (b) interference from adjacent crystals, (c) exhaustion of paraffin in solution, or (d) by evaporation of the solvent and excessive viscosity of the surrounding solution.

CRYSTALLIZATION UNDER OTHER CONDITIONS

It is again emphasized that the foregoing description of the growth of *n*-paraffin crystals applies only to crystallizations from solvent solutions on glass microslides at normal room temperatures which are below the transition and melting points of the compound. The description also applies only to reasonably pure individual or mixed *n*-paraffins, free of oils or other organic materials which inhibit or modify normal growth of the paraffins.

Under other conditions, the method of growth and the final crystal forms of the *n*-paraffins may be different from those we have described. For example, if during growth of a crystal the *c*-axis of the lattice is not parallel to the optical axis of the microscope, change in crystal dimensions may be visible during growth. When crystals are formed out of solvent solution at temperatures between the lower transition and melting points, the lattice may be warped, so that the *c*-axis lies at angles other than vertical. A common habit under these conditions is the formation of "needles." One type of paraffin needle is formed by a rolling up or curling of the {001} layers around the axis of the needle. During growth, these needles are seen to increase rapidly in length and more slowly in width as successive {001} layers are added to the elongate, cigar-shaped body. The long axes of such needles usually lie horizontally on the microslide. The {001} layers are wrapped around the needle in a manner which may be compared to a long stack of conical paper drinking cups, or to the wrapper leaves on a cigar. As viewed through the microscope, the *c*-axis of the distorted layers of the lattice approaches the horizontal position toward the lateral margins of the needle, and the vertical position toward the median or central portion of the needle. Thus the birefringence seen toward the two lateral margins of the needle is much stronger (γ–β) than that seen along the central axis of the needle (β–α). As observed between crossed nicols, such needles present a characteristic appearance of two bright zones along the margins of the needle, separated by a darker zone extending along the needle axis. Needles of this type are seen in *n*-paraffins which have crystallized from the melt, and sometimes in those crystallized from solvent solution at ordinary temperatures, but with oil, asphalt, or some other organic materials present in the solution as impurities.

The formation of needles of the type described, and many other variations of crystal form and habit have been described in various published papers on the subject (see Heck, 1936; Kolvoort, 1938; Gray, 1943; Rhodes *et al.*, 1927; Tanaka *et al.*, 1928; Ferris *et al.*, 1931). These numerous other crystal forms are rarely or never observed when reasonably pure individual or mixed *n*-paraffins are crystallized under a cover glass on a microslide at ordinary temperatures, employing such solvents as carbon tetrachloride, benzene, toluene, and xylene.

ACKNOWLEDGMENTS

The writer wishes to express his thanks to Professor Paul F. Kerr, who very kindly reviewed the manuscript of this paper and made many helpful suggestions; to Professor J. M. Nelson, who kindly reviewed the chemical phases of the paper; and to Dr. C. W. Sheppard for his interest in the work, and for supplying a sample of pure Octacosane. The writer assumes full responsibility for any errors that may exist;

REFERENCES

1. HECK, C. M., Note on discovery of spiral structure in paraffin crystals: *Science News Letter*, Dec. 12, 1936.
2. GRUSE, W. A., AND STEVENS, D. R., *The Chemical Technology of Petroleum*, 2nd. ed. (**1942**), McGraw-Hill, N. Y.
3. MÜLLER, ALEX, A further *x*-ray investigation of long chain compounds (n-hydrocarbon): *Proc. Royal Soc.*, A, **120** (June), 437–459 (1928).
4. MÜLLER, ALEX, The connection between the zig-zag structure of the hydrocarbon chain and the alternations in the properties of odd and even numbered chain compounds: *Proc. Royal Soc.*, A, **124** (April), 317–321 (1929).
5. MÜLLER, ALEX, The crystal structure of the normal paraffins at temperatures ranging from that of liquid air to the melting points: *Proc. Royal Soc.*, A, **127** (March), 417–430 (1930).
6. PIPER, S. H., CHIBNALL, A. C., HOPKINS, S. J., POLLARD, A., SMITH, J. A. B., AND WILLIAMS, E. F., Synthesis and crystal spacings of certain long-chain paraffins, ketones, and secondary alcohols: *Biochem. Journ.*, **25** (October), 2072–2094 (1931).
7. MÜLLER, ALEX, An *x*-ray investigation of normal paraffins near their melting points: *Proc. Royal Soc.*, A, **138** (July), 514–530 (1932).

8. Chibnall, A. C., Piper, S. H., Pollard, A., Williams, E. F., and Sahai, P. N., The constitution of the primary alcohols, fatty acids and paraffins present in plant and insect waxes: *Biochem. Journ.*, **28** (October), 2189–2208 (1934).
9. Chibnall, A. C., and Piper, S. H., The metabolism of plant and insect waxes: *Biochem. Journ.*, **28** (October), 2209–2219 (1934).
10. Kolvoort, E. C. H., Crystal twins of normal C_{24} H_{50} and the influence of phase transitions on their orientation: *Journ. Inst. Petroleum*, **24**, 338–347 (1938).
11. Gray, C. G., The phase transformations of normal paraffins: *Journ. Inst. Petroleum*, **29**, No. 236 (August), 226–234 (1943).
12. Rhodes, F. H., Mason, C. W., and Sutton, W. R., Crystallization of paraffin wax: *Ind. and Eng. Chem.*, **19**, No. 8 (August), 935–938 (1927).
13. Tanaka, Y., Kobayashi, R., and Ohno, S., Studies on crystallization of paraffin: *Journ. Faculty of Engineering, Tokio Imp. Univ.*, **17**, No. 15 (November), 275–292 (1928).
14. Ferris, S. W., Cowles, H. C., and Henderson, L. M., Composition and crystal form of the petroleum waxes: *Ind. and Eng. Chem.*, **23**, No. 6 (June), 681–688 (1931).

MAXIMUM ERROR IN SOME MINERALOGIC COMPUTATIONS

H. W. FAIRBAIRN AND C. W. SHEPPARD,
Massachusetts Institute of Technology, Cambridge, Mass.

CONTENTS

ABSTRACT........ 673
INTRODUCTION........ 674
DETERMINATION OF DENSITY........ 675
  SUSPENSION METHOD........ 675
  HYDROSTATIC METHOD........ 676
    Jolly balance........ 675
    Berman balance........ 676
  PYCNOMETER METHOD........ 678
  X-RADIATION METHOD........ 680
  COMPARATIVE ACCURACY........ 682
DETERMINATION OF REFRACTIVE INDEX........ 683
  MINIMUM DEVIATION METHOD........ 683
  GRAZING INCIDENCE METHOD........ 686
  UNIVERSAL STAGE EXTRAPOLATION METHOD........ 687
  OPTIC ANGLE METHOD........ 689
  COMPARATIVE ACCURACY........ 691
DETERMINATION OF BIREFRINGENCE........ 691
  GENERAL COMPENSATOR METHOD (Berek)........ 691
  EMMONS EXTRAPOLATION METHOD........ 693
  OPTIC ANGLE-COMPENSATOR METHOD........ 693
  COMPARATIVE ACCURACY........ 694
DETERMINATION OF OPTIC ANGLE........ 695
  COMPENSATOR METHOD........ 695
  REFRACTIVE INDEX METHOD........ 695
  EXTINCTION ANGLE METHOD........ 697
    Optic plane horizontal........ 697
    Optic plane vertical........ 699
  INTERFERENCE FIGURE METHODS........ 700
  COMPARATIVE ACCURACY........ 701
SUMMARY........ 702
ACKNOWLEDGMENTS........ 702

ABSTRACT

The notable lack of quantitative information regarding errors in many mineralogic computations has prompted the writers to construct a series of diagrams from which such information can be readily obtained. These include various determinative methods for density, refractive index, birefringence, and optic angle Assuming a skilled operator, maximum values of the error in single observations are assigned to each procedure, so that the diagrams represent "worst" values of error, rather than a "probable" error as determined from a series of observations. Comparison of the various procedures is based on this "maximum expected" error.

INTRODUCTION

It is a truism that all physical measurements are approximations which approach, in varying degree, an unattainable absolute value. As a result it is essential that the degree of approximation, or amount of fractional deviation, be adequately known. In the field of mineralogy everyone knows about this, but few have consistently done anything about it. For various reasons the subject as a whole has been treated in the manner of a poor relation, with much overstatement and some understatement of the fractional deviations obtained (Hey, 1933). The present paper is an attempt to improve this situation.

Deviations (also called uncertainties or errors) are classified as systematic (periodic) or random (accidental). Systematic errors are inherent in every experimental investigation (e.g. temperature variations in density and refractometric work) and can be controlled. This control is in some cases fine enough so that this type of error is negligible compared with the random error. Random deviations arise through reading of scales, adjustment of extinction positions, etc. For a single observation the uncertainty of the measurement depends in part on the skill of the observer, in part on the character of the apparatus. If repeated observations are made, the random error may be expressed quantitatively by calculating a "probable error." As there is a 50% probability of a measurement differing from the true value by more than this amount, the "probable error" of an observation may give a false impression of accuracy. In the present discussion "maximum expected error" is considered only—i.e., it represents the probable worst value which a skilled operator would obtain from a single measurement with a given apparatus. If it is known in advance how large this maximum expected error is likely to be and if this value, added to the known systematic error, gives a total uncertainty which can be tolerated for the work in hand, the labor of computing a standard "probable error" may be avoided. This maximum error is of course not a precise quantity, but the numerical values used in constructing the diagrams given here are believed to be large enough so that the curves give fractional deviations which would be exceeded only in rare instances.

The general method followed is (1) differentiation of the basic formula with respect to all pertinent variables, (2) assumption of maximum expected values for the differentials, (3) solution of the differential equation to determine the maximum expected random error, (4) calculation of the systematic error, (5) addition of random and systematic errors, (6) construction of a diagram.

It is assumed that the reader is familiar with the determinative methods under scrutiny and has acquired enough manipulative skill to avoid random errors appreciably greater than those shown in the diagrams.

In cases where the observer believes that the uncertainty in any of his own measurements differs markedly from the values used here, an adjusted diagram can usually be made with little labor by referring to the proper differential equation.

DETERMINATION OF DENSITY

Four commonly used methods of density determination are considered and their relative accuracies compared. The suspension, hydrostatic, and pycnometer procedures give relative density, or "specific gravity,"[1] whereas the x-radiation method measures density directly, without use of a reference fluid such as water or toluene.

SUSPENSION METHOD. Although this method does not involve any computation and is limited in its application, its potential accuracy is worthy of note, especially where Clerici's solution is used (Jahns, 1939). The random error in density inherent in Jahns' refractive index-density curve is given as .01. A second random error arises from reading the Abbé refractometer, and may be assumed to be .0005. Using the slope of this curve to obtain the ratio of density and index change (dD/dn), the uncertainty in density is found to be .00044, negligible in comparison with the first random error. The total random error of .0104 is converted to a fractional deviation dD/D, this value being plotted against D in Fig. 2 (inset, top left). It is assumed that the systematic error arising from temperature variations can be adequately controlled.

Extension of the density range through use of a glass float (of known weight and density) attached to the mineral fragment can be achieved, but with relative loss in accuracy. This case is not considered here (see Bannister and Hey, 1937).

HYDROSTATIC METHOD. A number of methods of this type have been described, of which two are discussed here.

Jolly Balance. The expression for density is

$$D = \frac{W_A D_W}{W_A - W_W},$$

where W_A = weight of substance in air.

W_W = weight of substance in water.

D_W = density of water at room temperature relative to $D_W = 1$ at 4°C.

---

[1] Although widely used, "specific gravity" is terminologically incorrect as a synonym for relative density, and is physically incorrect as a synonym for density determined by the x-radiation method. "Gravity" implies the weight of a body, i.e., the earth's attraction for it, which is not an intrinsic property, whereas by definition density is the mass of a body per unit volume, the mass being an intrinsic and invariable property.

The fractional deviation is given by

$$\frac{dD}{D}=\frac{W_A dW_W + W_W dW_A}{W_A(W_A - W_W)}+\frac{dD_W}{D_W},$$

where dW_W and dW_A are the uncertainties in determination of W_A and W_W, respectively, and dD_W is the uncertainty in density of water at any temperature. As dW_A and dW_W are obviously equal they may be replaced by dW. Furthermore, the uncertainty in D_W is relatively negligible so that, finally,

$$\frac{dD}{D}=\frac{dW(W_A + W_W)}{W_A(W_A - W_W)},$$

which represents the fractional deviation arising from the random errors of reading the scale. The obvious source of systematic error would be temperature variations which would affect the density of the water. However, it is found that, between 15° and 25°C. (room temperature range), this error may be neglected.

Figure 1 has been prepared from data obtained with the current apparatus offered by the Central Scientific Company. Two springs are provided to extend the range of the balance. The uncertainty of any individual reading of the scale should not exceed one-quarter of a division. In order to compare directly with errors found in the other weighing methods, the springs were calibrated in grams, giving $dW=.005$ gm. for the light spring, and $dW=.025$ gm. for the heavy spring.[2] This conversion is of course not ordinarily necessary. Per cent fractional deviation is plotted against density for each spring, using four values of W_A known to be within the range of the scale. The sensitivity of each spring is considered constant within the range selected. It is seen from Fig. 1 that least accuracy (greatest fractional deviation) is obtained where W_A is low and D is high, and, conversely, that maximum accuracy is to be expected from the combination of high W_A and low D. Furthermore, the variation in dD/D with D is much less for high W_A than for low W_A. These observations hold also, in varying degree, for the other balance methods discussed (Figs. 2 and 3).

Berman Balance. As with the Jolly balance the fractional deviation is

$$\frac{dD}{D}=\frac{dW(W_A + W_W)}{W_A(W_A - W_W)}+\frac{dD_T}{D_T},$$

where dD_T and D_T refer to toluene instead of water. At any given temperature there is an uncertainty $dD_T = .0005$ in the density of toluene (Timmermans, 1912). The random error dW of a single scale reading on

---

[2] Figure 1 will probably require some adjustment for Jolly balances of different make.

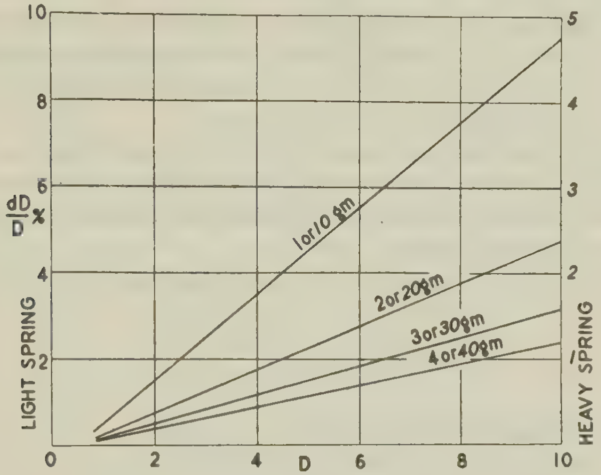

Fig. 1. *Jolly balance.* Variation in accuracy for different densities. Random error computed for W_A values of 1, 2, 3, 4 gm. (using light spring) and 10, 20, 30, 40 gm. (using heavy spring). Based on an error of .25 division in reading the scale.

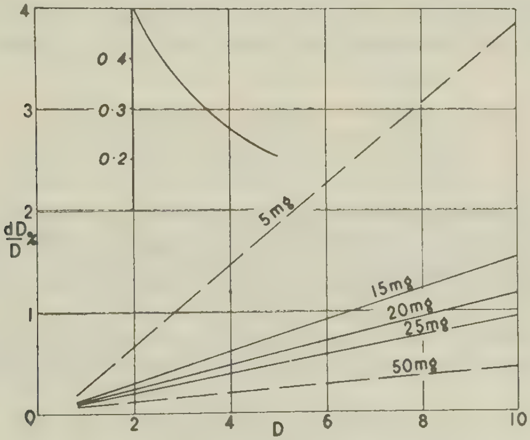

Fig. 2. *Berman balance and* (*inset, top left*) *Clerici solution method* (*Jahns*). Random error for Berman balance computed for W_A values of 5, 15, 20, 25, 50 mg. Based on dW = .01 mg. Full lines (15, 20, 25 mg.) cover the range of maximum sensitivity of the balance as specified by the manufacturer. Random error for Clerici solution method based on experimental data given by Jahns (1939).

the balance should not exceed .01 mg. The systematic error arising from determinations made at various temperatures is relatively negligible in the range 15°–25°C. Surface tension deviation may also be neglected where the suspension wire diameter is a small fraction of millimeter. Figure 2 is therefore constructed directly from the equation given above. Optimum conditions of accuracy are realized only for W_A values from 15 to 25 mg., as specified by the manufacturer.

Where a determination is made with several small fragments instead of with a larger, single piece, accuracy will probably be lowered because of less perfect wetting. Unlike the pycnometric method, this systematic error can not be eliminated.

Pycnometer method. Density by the pycnometer procedure is given by

$$D = \frac{(W_2 - W_1)D_T}{W_2 - W_3 + D_TV}$$

where W_1 = weight of pycnometer
W_2 = weight of pycnometer + powder
W_3 = weight of pycnometer + powder + toluene
D_T = density of toluene
V = volume of pycnometer.

If a silica-glass pycnometer is used, the uncertainty in V may be reduced by careful calibration to a relatively negligible value (Ellsworth, 1928). In the following expression for fractional deviation V is therefore considered constant

$$\frac{dD}{D} = \frac{2dW}{W_2 - W_1} + \frac{dD_T}{D_T}\left(\frac{W_2 - W_3}{W_2 - W_3 + D_TV}\right).$$

The three uncertainties dW_1, dW_2, dW_3 used in the first step of the differentiation are equal and have been replaced by dW in the final condensed expression above.[3] As the uncertainty in weighing on the ordinary

---

[3] As the writers have not succeeded in duplicating the expressions derived by one or two other authors for the pycnometric method, the derivation used here is given in detail.

$$D = \frac{(W_2 - W_1)D_T}{W_2 - W_3 + D_TV}.$$

Taking logarithms of each side,

$$\log D = \log D_T + \log (W_2 - W_1) - \log (W_2 - W_3 + D_TV).$$

Differentiating,

$$\frac{dD}{D} = \frac{dD_T}{D_T} + \frac{dW_2 - dW_1}{W_2 - W_1} - \frac{dW_2 - dW_3 + VdD_T}{W_2 - W_3 + D_TV}.$$

chemical balance should not exceed .0001 gm., this value is assigned to dW in constructing Fig. 3. $dD_T = .0005$ as in Fig. 2. Room temperature variations produce relatively negligible systematic errors. The 10 cc. bottle described by Ellsworth (1928) is used to show variations in accuracy for powder samples weighing 1, 2, 5, and 10 gm.; the 0.1 cc. bottle described by Winchell (1938) is used similarly for powder weights of 0.1, 0.2, and 0.5 gm.

Every precaution must be taken to wet the powder thoroughly, as failure to remove all the imprisoned air will lead to deviations much greater than the random error from weighing. Ksanda and Merwin (1939) have described an excellent technique of this kind.

Figure 3 shows that bottles of large capacity give smaller fractional deviations over the usual range of powder weights than do bottles of small volume, assuming equivalent conditions of weighing. This becomes obvious from inspection of the differential equation. Increase in V reduces the dD_T/D_T term, and increase in $W_2 - W_1$ (weight of powder in air) reduces the dW term. Offsetting this apparent superiority of the larger bottle, however, is the fact that its greater bulk of powder increases the

---

Collecting the dW_1, dW_2, dW_3, and dD_T terms separately,

$$\frac{dD}{D} = dD_T\left(\frac{1}{D_T} - \frac{V}{W_2 - W_3 + D_TV}\right) - dW_1\left(\frac{1}{W_2 - W_1}\right) + dW_2\left(\frac{1}{W_2 - W_1} - \frac{1}{W_2 - W_3 + D_TV}\right) + dW_3\left(\frac{1}{W_2 - W_3 + D_TV}\right)$$

For determination of *maximum* error all the bracketed expressions must have the same sign. The dW_1 term is therefore made positive. (The minus signs *within* the dD_T and dW_2 brackets must be left unchanged, as D_T and W_2 occur in both numerator and denominator of the original density equation. Errors in their measurement would therefore be expected to compensate each other partially, as shown by the minus signs in the differential equation.) Furthermore, as $dW_1 = dW_2 = dW_3$, we replace each by dW. Thus

$$\frac{dD}{D} = dD_T\left[\frac{W_2 - W_3}{D_T(W_2 - W_3 + D_TV)}\right] + dW\left[\frac{(W_2 - W_3 + D_TV) + (W_2 - W_3 + D_TV) - (W_2 - W_1) + (W_2 - W_1)}{(W_2 - W_1)(W_2 - W_3 + D_TV)}\right]$$

$$= dD_T\left[\frac{W_2 - W_3}{D_T(W_2 - W_3 + D_TV)}\right] + dW\left[\frac{2}{W_2 - W_1}\right]$$

If V is not considered constant the term $\left[\frac{D_TdV}{W_2 - W_3 + D_TV}\right]$ must be added to the above.

difficulty of removing the last traces of trapped air. Homogeneity in composition of the sample is also more difficult to attain with a large sample. It is probable therefore that in practice the accuracy of the two bottles will be about the same.

In the micropycnometric procedure described by Bannister and Hey (1937) only 15 to 25 mg. of sample are required, with a reported accuracy of 0.5%. As part of this error stems from an uncertainty in the volume of liquid used, a greater error than that of Fig. 3 would be expected.

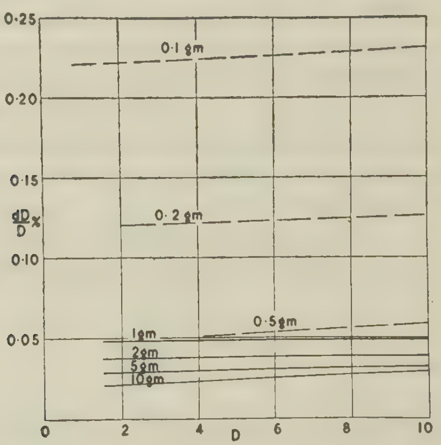

FIG. 3. *Pycnometer method*. Variation in accuracy for different densities. Random error for 10 cc. bottle (Ellsworth type) and .1 cc. bottle (Winchell type). Full lines refer to the 10 cc. bottle for mineral weights (in air) of 1, 2, 5, 10 gm.; broken lines refer to the .1 cc. bottle for mineral weights (in air) of .1, .2, .5 gm. Based on $dW=.0001$ gm. and $dD_T=.0005$.

However, uncertainties regarding the homogeneity and wetting of the powder may be better controlled in the Bannister-Hey method than in the others, and too much emphasis should not be placed therefore on the purely mathematical aspects of the case.

X-RADIATION METHOD. Density by this method is expressed by

$$D = \frac{MZ}{AV}$$

where M = molecular weight of the material
Z = number of formula-units in a unit cell
V = volume of unit cell
A = Avogadro's number (6.02×10^{23}).

As V is the single variable,[4]

$$\frac{\Delta D}{D} = -\frac{\Delta V}{V}.$$

In a cubic crystal, $a_0 = d(h^2+k^2+l^2)^{1/2}$
where a_0 = length of side of unit cell,
d = interplanar spacing of planes with indices *hkl*.

Therefore $\frac{\Delta a_0}{a_0} = \frac{\Delta d}{d}$ But $\frac{\Delta V}{V} = \frac{\Delta(a_0^3)}{a_0^3} = \frac{3(\Delta a_0)}{a_0} = \frac{3\Delta d}{d}$

From Bragg's equation $d = \lambda/2 \sin\theta$,
where λ = wave length of *x*-radiation used,
θ = diffraction angle.

The fractional deviation of d is $\Delta d/d = -\cot\theta\Delta\theta$. Expressing the fractional deviation in density in terms of the diffraction angle, $\Delta D/D = 3 \cot\theta\Delta\theta$ (for cubic crystals only).

Application of this equation is confined here to powder photography. The error in reading a millimeter scale placed on a line of the film should not exceed .25 mm. for any single measurement. Therefore the uncertainty in the distance between such a line and its mate on the other side of the line of zero diffraction is 0.5 mm. As this total distance in a camera of 57.3 mm. diameter is equivalent to 4θ, the error in θ is .125°. That is, $\Delta\theta = .125/57.3 = .00128$ radians. The curve R for random error in Fig. 4 is based on this value.

The four systematic errors inherent in *x*-ray crystal diffraction work—absorption of radiation by the specimen, eccentricity of the sample with respect to the camera, film shrinkage after development, and uncertainty in the camera radius—must each be considered on its merits. As details are given by Buerger (1942) for such corrections the matter is taken up only briefly here. Use of a two-hole film (Straumanis method) permits the camera radius and film shrinkage errors to be combined, and for a carefully constructed camera and film dried at room temperature, the error from this source is relatively negligible. It does not appear in Fig. 4.

The eccentricity error is small but appreciable. Its curve (E in Fig. 4) is based on a maximum expected displacement of the sample relative to the true center of the camera of .025 mm. The equation used is given by Buerger (1942, p. 413). The deviation may be positive or negative.

---

[4] To avoid confusion with the interplanar spacing symbol *d*, Δ replaces here the customary differential symbol.

The absorption error (Buerger, 1942, p. 414) is based on complete absorption, a specimen diameter of .25 mm., a pin-hole—specimen distance of 10.6 mm., and camera diameter 57.3 mm. Its curve (A in Fig. 4) shows an order of magnitude for $\Delta D/D$ similar to the curve R, and of the same sign.

The total value of the maximum expected error is shown by curve T and has been drawn using positive values for the individual errors. As the random error may be opposite in sign to the absorption error, and is of the same order of magnitude, the total error may, however, be very small. Curve T represents the worst possible case. The diagram does not include values smaller than 50°, as the accuracy decreases very rapidly in this range.

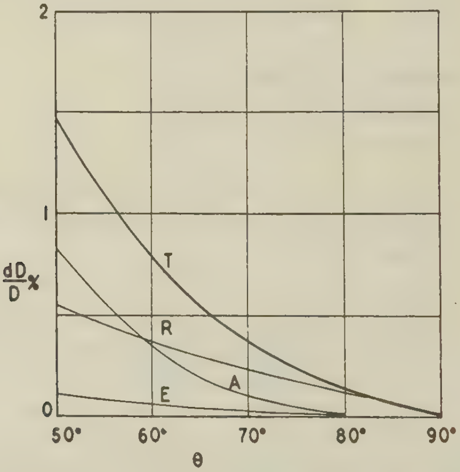

FIG. 4. *X-ray method.* Variation in accuracy for different diffraction angles. Random error (curve R) based on an uncertainty of .25 mm. in reading the position of a diffraction line. Absorption error (curve A) from data in Buerger (1942). Eccentricity error (curve E) likewise from data in Buerger (1942). Curve T shows total error where R, A, E are assumed to have the same sign.

COMPARATIVE ACCURACY. Excluding the x-ray method, comparison of the remaining procedures shows that the pycnometer method has the greatest inherent accuracy, the Jolly balance method the least. Choice of method is dictated by the nature of the material and the degree of accuracy required. For most work the accuracy range of the Berman balance is adequate, provided that a single fragment of suitable weight can be obtained.

Direct comparison of these weighing methods with the x-radiation method is not possible, as the latter gives the density of the unit cell whereas the former give values for aggregates of unit cells. The individual cells in these aggregates are rarely, if ever, packed together perfectly, with the result that lower density values are obtained than from the *x*-ray procedure. If it is desired to contrast the two density values for a given material, a weighing method should be selected which gives an accuracy comparable with that indicated by the θ value chosen in Fig. 4. In general, the Berman balance would satisfy this requirement.

Determination of Refractive Index

As this paper is concerned with errors in computation only, the accuracy of direct-reading instruments will not be discussed. In the case of refractometers the accuracy of the widely used Abbé type has recently been reviewed by Tilton (1942) in an informative paper. It need only be stated here that the ordinary Abbé used in mineralogical laboratories reads correctly to ±.0002 in its lower range, but is considerably less accurate in its upper range. Other direct-reading refractometers (Fisher, Nichols, etc.) are usually reliable to ±.001.

Minimum deviation method. In the field of precise refractometry the minimum deviation method is preferable to any other. Where moderate precision is required, as in standardization of oils or melts for use in the immersion method of refractive index determination, it affords the only universal method for the entire range of indices. The accuracy of the method has been discussed by Tilton (1935) who lists 19 sources of error for determinations of the highest precision (±.000001). As mineralogists seldom require this accuracy for crystal measurement, and never for immersion oils or melts, only the random error of reading prism and minimum deviation angles need be considered here.

The index of refraction is given by

$$n = \frac{\sin \dfrac{A + D_m}{2}}{\sin \dfrac{A}{2}},$$

where A = angle of the prism.

D_m = minimum deviation angle.

Differentiating partially with respect to A, $dn = -1/2 \sin D_m/2 \operatorname{cosec}^2 A/2 \, dA$, and partially with respect to D_m, $dn = 1/2 (\cos D_m/2 \cot A/2$

$-\sin D_m/2)\,dD_m$. As it is probable[5] that $dA = dD_m$, we replace each by dr, so that the total random error is

$$\Sigma(dn) = \frac{1}{2}\left[\operatorname{cosec}\frac{A}{2}\cos\frac{A+D_m}{2} - \operatorname{cosec}^2\frac{A}{2}\sin\frac{D_m}{2}\right]dr.$$

In constructing Fig. 5 the error in the prism and minimum deviation angles is assumed to be ±1′, so that $dr = .000291$ radians. The second term in the differential equation is considered positive in order to give dn its maximum expected value.[6] Most single determinations will have greater accuracy than that indicated by the graph. In working with crystal prisms the deviation is likely to be much less than 1′, but with the ordinary hollow cell used for oil determinations this is unlikely, and for crude prisms composed of S-Se mixtures may be much greater than 1′.

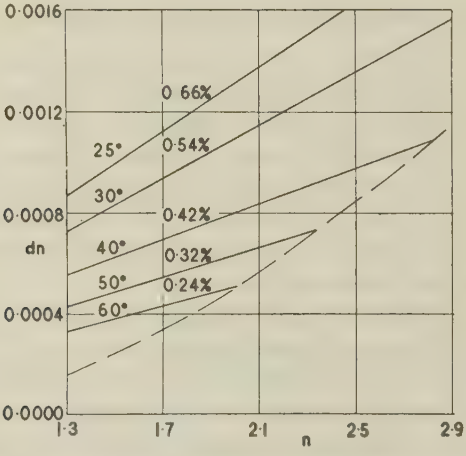

FIG. 5. *Minimum deviation method.* Variation of random error in *n* for a series of *n* values. Computations shown for prism angles of 25°, 30°, 40°, 50°, 60°, with the % accuracy given for each. Steep curve transecting the prism curves is the locus of limiting values of prism angles for determination of a given refractive index. Diagram based on an uncertainty of ±1′ in determination of prism and minimum deviation angles.

Figure 5 shows the total maximum expected error for prisms of varying angle over a wide range of indices. For a given index greatest accuracy (least dn/n%) is attained where large prisms are used. Inspection of the formula

---

[5] This may not be true if the prism angle is determined from readings of the table circle, and the minimum deviation angle from readings of the telescope circle. The table angles of small spectrometers and goniometers tend to be less accurate than telescope angles. However, if the prism angle is determined by the split-beam method, no table angle need be used, and except in high-precision work gives very satisfactory results (Guild, 1923).

[6] The small numerical range of the common refractive indices makes it unnecessary to plot the variation in fractional deviation for different values of *n*.

$$n = \sin\frac{A + D_m}{2} \Big/ \sin\frac{A}{2}$$

indicates a maximum value of n for any given prism angle. The boundary curve in Fig. 5 shows this graphically. For example, the limiting refractive index determinable with a 60° prism angle is 2.0. In practice, since the proportion of transmitted light at grazing incidence is greatly reduced relative to the reflected portion, it is never possible to proceed to the limit shown in the diagram.

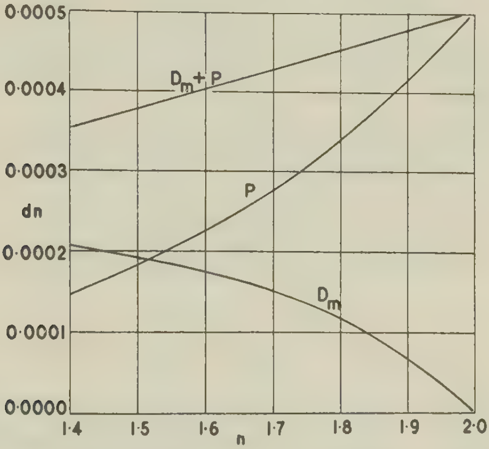

FIG. 6. *Minimum deviation method where prism angle is* 60°. Curve P shows random error arising from prism angle uncertainty of 1′. Curve D_M shows random error arising from minimum deviation uncertainty of 1′. Upper curve shows the total error where P and D_M are assumed to have the same sign.

Figure 6 gives greater detail for a 60° prism. Curve P shows the variation in prism angle error for various indices; D_m shows dn for different indices arising from measurement of the minimum deviation angle. At the limiting index of 2.0 the prism angle error reaches its maximum whereas the minimum deviation error becomes zero. The upper, straight line represents the total maximum expected error. If the Gifford method[7] is used, the error in prism angle becomes negligible and the total uncertainty is shown by D_m. In all cases where the demands of this method can be met, increased accuracy will result, particularly for refractive indices approaching 2.0 in magnitude.

---

[7] This method (Gifford, 1902) makes use of a closed prism whose angles approximate 60°. Minimum deviation angles are measured across each prism and an average computed. Angle A may then be assumed equal to 60° without any accurate measurement of the individual prisms. An uncertainty in A of the order of magnitude of 1° causes an uncertainty of only ±.0001 in n. As there need be no difficulty in maintaining the prism deviations at much less than 1°, the resultant prism angle error using this method becomes negligible.

Where the goal of accuracy is in the neighborhood of ±.0001, systematic errors become significant only for determinations made on liquids. Temperature corrections are necessary, particularly for methylene iodide and mixtures containing it, and require control to at least 0.1°C. if the index error limit of .0001 is to be maintained. In addition the hollow cell must be constructed of optically flat glass. Suitable material may be selected according to the method suggested by Larsen and Berman (1934). In Figs. 5 and 6 it is assumed that these systematic errors can be reduced to negligible proportions and that only random errors remain.

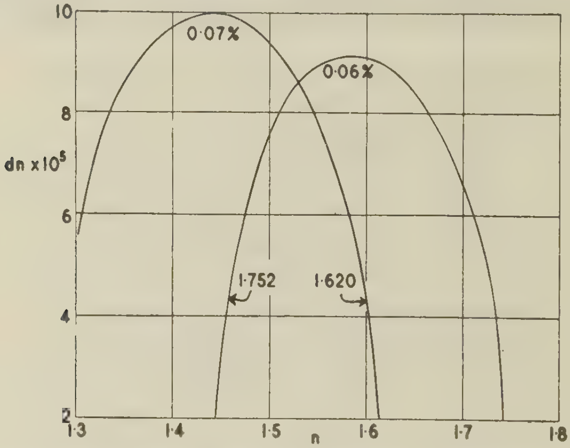

FIG. 7. *Grazing incidence method* (*Pulfrich refractometer*). Variation in dn with n shown for two prisms of refractive index as marked. Approximate % accuracy at curve maxima is also given. Based on an uncertainty of ±1′ in reading the scale.

GRAZING INCIDENCE METHOD. This method is incorporated in the widely used Pulfrich refractometer. Although less used by mineralogists than by chemists (Gibb, 1942, p. 333), and inherently less accurate than instruments used for precise minimum deviation work, a brief comparison is not out of place. Refractive index is given by

$$n = (n_p^2 - \sin^2 r)^{1/2}$$

where n_p = refractive index of prism,
r = angle read on divided circle.

Differentiation gives

$$dn = -\left[\frac{\sin 2r}{2(n_p^2 - \sin^2 r)^{1/2}}\right]dr.$$

The error in a single reading in the middle range of r values is not likely to exceed 1′, so that dr = .000291 radians. Figure 7 shows a graphical solution of the differential equation for two prisms of $n = 1.620$ and $n = 1.752$. For each prism there is an r value which gives maximum fractional deviation (.07% and .06% as indicated). Thus for material of $n = 1.6$ the maximum expected error would be only about one-half as great where the lower index prism is used as where the higher one is used. For high and low r values, however, dr may easily exceed the value used in the diagram, so that the accuracy indicated in the lower part ($dn < .00004$) may not be realized. However, even the worst values at the noses of the curves are as good, or better, than the accuracy to be expected from ordinary four-figure minimum deviation measurements.

UNIVERSAL STAGE EXTRAPOLATION METHOD. In cases where one critical index alone can be determined in a given oriented optic symmetry plane, measurement of an intermediate index at a known angle in this plane makes possible the computation of the other critical index. This method, first used by Pauly (Johannsen, 1918, p. 266), and later developed by Emmons (1943, pl. 10) depends on the following equation

$$n_x = \frac{n_2(n_1^2 \sin^2 \phi + n_x^2 \cos^2 \phi)^{1/2}}{n_1},$$

where n_x = unknown critical index,
n_1 = known critical index,
n_2 = intermediate index,
ϕ = rotation angle used in obtaining n_2.

Assuming that the uncertainties in n_1 and n_2 are the same, and using dn to represent both, the differential equation is:

$$\frac{dn_x}{n_x} = \left[\frac{1}{n_2} + \frac{n_x^2 \cot^2 \phi}{n_2^2}\left(\frac{1}{n_2} - \frac{1}{n_1}\right)\right] dn + \left(1 - \frac{n_x^2}{n_1^2}\right) \cot \phi d\phi.$$

If $dn = .001$ and the uncertainty[8] in ϕ is 1° ($d\phi = .0174$ radians), the equation appears graphically as in Fig. 8. It is assumed that $n_1 > n_x$. In Fig. 8 dn_x is plotted against (n_1-n_x) for different values of ϕ using the computations made for $n_1 = 1.6$. For other values of n_1 no appreciable difference in the deviations is obtained. For $\phi = 90°$ inspection of the differential equation shows that $dn_x = (n_x/n_2)$ dn and since n_2 now equals n_x, then $dn_x = dn = .001$ as shown in Fig. 8. The total dn term remains fairly constant at .001+, most of the variation being shown by the dϕ term. In general, dn_x is least where large angles are combined with low partial birefringence. Except for angles of less than 20°, however, dn_x changes little where partial birefringence is low.

---

[8] The uncertainty in ϕ stems from the initial random error in orienting the optic symmetry plane rather than from any inherent defect in the OEW axis of the stage.

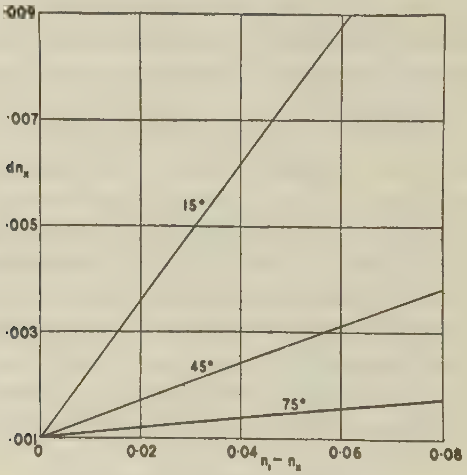

FIG. 8. *Extrapolation method.* Variation in dn_x for different partial birefringence ($n_1 - n_x$). Shown for three values of ϕ, where $n_1 = 1.6$. Based on dn = .001 and an uncertainty in ϕ of 1°.

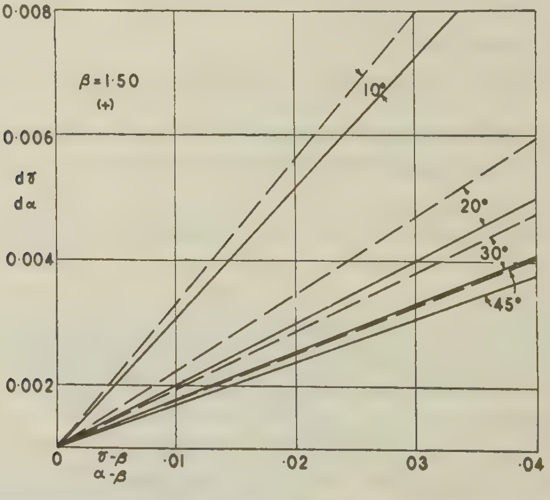

FIG. 9. *Optic angle method.* Variation in dγ (or dα) for different values of $\gamma - \beta$ (or $\alpha - \beta$). Four selected values of the optic angle are used. Diagram based on $\beta = 1.50$ and an optically positive crystal. Full lines refer to dα only; broken lines to dγ. The uncertainty in determination of the known refractive indices is .001 and in the optic angle 1°.

If $n_1 < n_x$, dn_x increases by a few per cent for high n_x and birefringence values; for low values the change is inappreciable. No diagrams for this case have been constructed.

OPTIC ANGLE METHOD. Mertie's nomogram (Mertie, 1942) showing the relations between α, β, γ, and V, based on ellipsoid geometry, is a necessary prerequisite to the deviation diagrams of this paper. As differentiation of the full equation gives a long, involved expression, the approximate equations

$$\sin^2 V = \frac{\beta - \alpha}{\gamma - \alpha} \text{ for optically positive substances,}$$

$$\sin^2 V = \frac{\gamma - \beta}{\gamma - \alpha} \text{ for optically negative substances,}$$

are used here. Differentiation of these with respect to α, β, γ in turn, gives

$$\left.\begin{aligned} d\alpha &= dn + \frac{(\beta - \gamma) \sin 2V dV}{\cos^4 V} \\ d\gamma &= dn + \frac{(\beta - \alpha) \sin 2V dV}{\sin^4 V} \end{aligned}\right\} \text{ for optically positive substances.}$$

$$\left.\begin{aligned} d\alpha &= dn + \frac{(\beta - \gamma) \sin 2V dV}{\sin^4 V} \\ d\gamma &= dn + \frac{(\beta - \alpha) \sin 2V dV}{\cos^4 V} \end{aligned}\right\} \text{ for optically negative substances.}$$

$$d\beta = dn + (\gamma - \alpha) \sin 2V dV \text{ for either positive or negative substances,}$$

where dn substitutes for $d\beta$ and $d\gamma$, $d\beta$ and $d\alpha$, $d\alpha$ and $d\gamma$, respectively, and is assumed equal to .001. The uncertainty in direct measurement of 2V need not exceed ±1° if both optic axes are found. If only one axis can be oriented the uncertainty will be ±2°. For low to moderate refringence and birefringence

$$d\alpha(+) = d\gamma(-) \quad \text{and} \quad d\gamma(+) = d\alpha(-).$$

Figure 9 is based on a constant value of $\beta = 1.50$, an optically positive substance and $dV = .0174$ radians (uncertainty in V of ±1°). It shows the variation in $d\alpha$ with change in α-β, and the variation in $d\gamma$ with change in γ-β, for selected values of V. As would be expected, the closer α (or γ) approaches β the smaller is $d\alpha$ (or $d\gamma$). The rate of increase in $d\alpha$ (or $d\gamma$) is greater for small V values than for large. The percent fractional deviation (accuracy) follows the same trend. Figure 10 is similar to 9, but is based on $\beta=1.90$. The same type of variation persists, but $d\alpha$ and $d\gamma$ are on the whole several times larger. For β values other than 1.50 and 1.90 interpolation or extrapolation will give a reasonably good result.

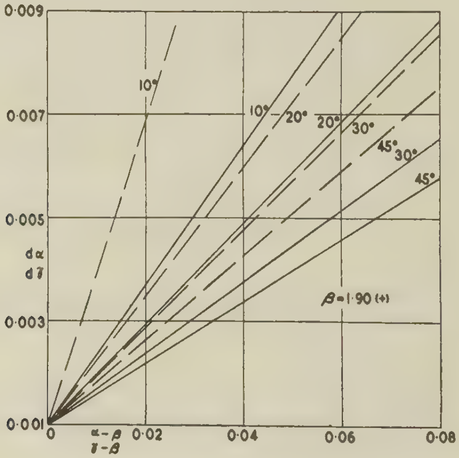

FIG. 10. *Optic angle method.* Same as Figure 9, but based on $\beta=1.90$.

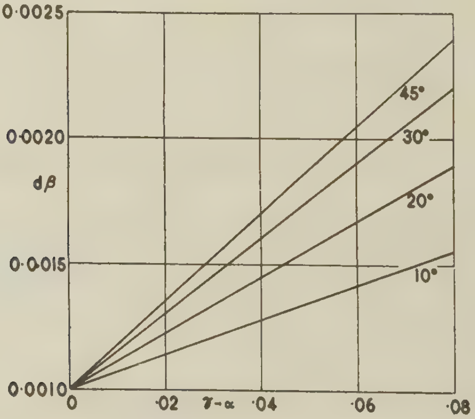

FIG. 11. *Optic angle method.* Variation in $d\beta$ for different values of total birefringence $(\gamma-\alpha)$. Four selected values of the optic angle are used. Based on uncertainties of .001 in determination of the known refractive indices, and of 1° in the optic angle.

Figure 11 is of similar form, but the variation is simpler in character. The curves are valid for any value of β, and for both positive and negative substances. In contrast with Figs. 9 and 10, $d\beta$ is smaller for small V values than for large. The overall range of $d\beta$ is also considerably less than for $d\alpha$ and $d\gamma$.

If the refractive indices are determined by precision methods, dn will be much less than .001. However, as the immersion method is rapid and widely used, the diagrams have been constructed for $dn = .001$.

COMPARATIVE ACCURACY. It has already been pointed out that the minimum deviation method is capable of greater precision than any other. However, the small spectrometers used for this method in most laboratories give results which are usually less accurate than those obtained with the Pulfrich refractometer, although adequate for practically all mineralogic work.

In contrast, the extrapolation and optic angle methods, insofar as they depend on immersion in oils, are much less accurate, giving third decimal place accuracy only.

DETERMINATION OF BIREFRINGENCE

GENERAL COMPENSATOR METHOD (*Berek*). Determination of refractive indices to ±.001 (immersion method) yields birefringence values accurate to ±.002. This direct method may be compared with an indirect method which makes use of the Berek compensator. Birefringence is determined by:

$$B = \frac{\Gamma'}{t/\cos\theta'}$$

where Γ' = retardation in the unknown for a particular orientation.

t = thickness of thin section.

θ' = angle between path of light and normal to the thin section.

By differentiation, $dB/B = d\Gamma'/\Gamma' - \tan\theta' d\theta' - dt/t$. The thickness t is found from a reference mineral of constant B (e.g. quartz), and $t = \Gamma'' \cos\theta''/B$, where Γ'' and θ'' are analogous to Γ' and θ'. Differentiating, $dt/t = d\Gamma''/\Gamma'' - \tan\theta'' d\theta''$. By substitution in the original dB/B equation, and assuming positive values for each term (to give the maximum deviation)

$$\frac{dB}{B} = \frac{d\Gamma'}{\Gamma'} + \tan\theta' d\theta' + \frac{d\Gamma''}{\Gamma''} + \tan\theta'' d\theta''$$

A general expression for $d\Gamma'/\Gamma'$ and $d\Gamma''/\Gamma''$ may be obtained from the basic compensator formula, $\log\Gamma = \log C + \log f(i)$ where C = constant of the compensator;[9] f(i) = function of angle of rotation i of compensator drum. As $f(i) = \sin^2 i + .204 \sin^4 i + \cdots$ for a calcite compensator (Berek, 1913), differentiation of the compensator formula gives:

---

[9] This constant must be determined for each instrument.

$$\frac{d\Gamma}{\Gamma} = \frac{\sin 2i(1 + .408 \sin^2 i)di}{\sin^2 i + .204 \sin^4 i}.$$

The maximum expected uncertainty of a single reading of the compensator drum is assumed to be 0.2°. The uncertainty in 2i would then be 0.4° and for i would be 0.2°. Then $di = 0.2/57.3 = .00349$ radians. Curve $d\Gamma/\Gamma$ in Fig. 12 shows the per cent variation in fractional deviation with change in Γ.[10] It is seen that accuracy is much increased where Γ is not too small.

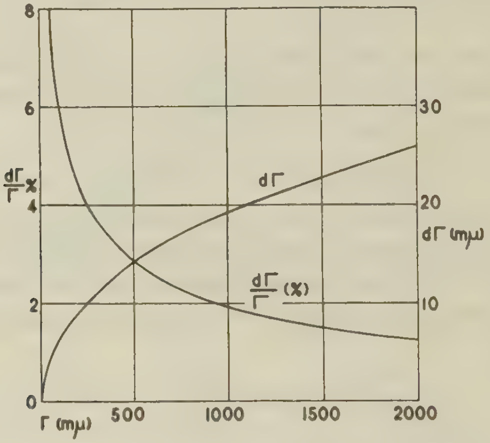

FIG. 12. *Berek compensator.* Variation in dΓ, and % accuracy of Γ, for different values of Γ. Based on an uncertainty of ±.2° in reading the compensator drum.

The uncertainties in θ' and θ'' may be assumed equivalent. Their magnitude depends on (1) error made in orienting the sections, (2) error in obtaining θ' and θ'' on the stereographic net, (3) error in the final hemisphere correction. Error 3 applies only to the unknown, as the refractive indices of the reference mineral are known. For the worst case, therefore, a maximum uncertainty of ±2° is not improbable. Where θ' and θ'' are both small, however, errors 2 and 3 will be negligible and the uncertainty should not exceed ±1°. The general importance of small θ values is indicated clearly in Fig. 13.

No simple diagram will show the variation in accuracy of B, but the total fractional deviation in any given case can be found by adding the values of the four terms in the equation for dB/B.

---

[10] The values in Fig. 10 are about double those given by Berek (1924, Fig. 22, p. 46). His calculation, however, is of a "mean" error, not a maximum expected deviation.

The preceding discussion implies strict uniformity in thin section thickness. As this condition is seldom realized, and, as it is physically impossible for the reference mineral and the unknown to occupy the same area of the section, a systematic error is thereby introduced which has not yet been considered. In the case of a strongly wedge-shaped section, detection by means of interference colors is easy, and the mount discarded if necessary. The thickness of apparently uniform sections can be rapidly checked by orienting three or four widely separated reference grains and noting the discrepancy in thickness obtained. Where this is small, e.g., .002 mm. across the whole section, it can be shown that, if unknown and reference mineral lie reasonably near to each other, a negligible error in B will result. In the case of mineral fragment mounts a reference mineral can always be added, so that close spatial association with the unknown is realized without difficulty.

In summary the accuracy of the indirect method increases where (1) thick rather than thin sections are used, (2) measurements are made on grains requiring the least angular rotation for their orientation, (3) the reference grain is as close as possible to the unknown.

Emmons extrapolation method. A new procedure described by Emmons (1943, plate 13), based on the Biot-Neumann equation, permits determination of total birefringence in any crystal where the optic plane is vertical. The compensator used may be of fixed retardation (standard gypsum or mica plate) or variable (Berek, graduated wedge, etc.). As the analytical work on which Emmons' plate 13 is based has not been published, no diagram of maximum error appears in this paper. Comment on the probable accuracy of the method will be found in the following section.

Optic angle-compensator method. The approximate relation

$$B_T = \frac{B_P}{\sin\theta \sin\theta'}$$

developed by Biot and Neumann (Johannsen 1918, p. 351), where B_T = total birefringence of the crystal, B_P = partial birefringence (as measured on a randomly oriented crystal section), θ and θ' are the angles subtended by each optic axis with the normal to the crystal section, becomes $B_T = (B_P/\sin^2 V)$ where the optic plane is parallel to the microscope axis, with X or Z vertical, thus making $\theta = V = \theta'$. A graphical solution of this equation is given by Emmons (1943, plate 11). Where $B_T > 0.1$ there will be an appreciable correction to apply to V (see Larsen and Berman, 1934, Fig. 1, or Emmons, 1943, plate 13). By differentiation,

$$\frac{dB_T}{B_T} = \frac{dB_P}{B_P} - 2 \cot V dV.$$

dB_P/B_P consists of four terms as described for the general compensator method (Figs. 12 and 13). The additional term 2cotVdV is shown graphically in Fig. 13 for two values of dV. The uncertainty in measuring an optic axis position need not exceed ±1°; therefore if both axes can be measured directly, the error in 2V is ±2° and in V is ±1°. If, however, only one axis position can be measured, the uncertainty in V is ±2°. Both these cases are included in Fig. 13. It is obvious that 2cotVdV is least where V is large and that the method fails badly for small V values.

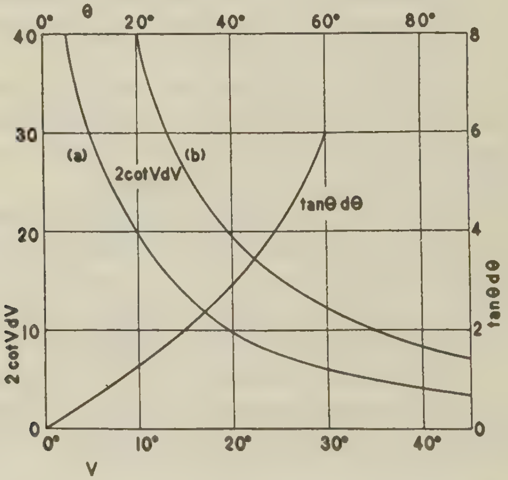

FIG. 13. *Trigonometric terms used in the compensator methods.* Tan θdθ curve (general compensator method) based on an error of ±2° in θ. 2 cot VdV curves (optic angle-compensator method) based on an uncertainty in V of ±1° in curve (a) and of ±2° in curve (b).

COMPARATIVE ACCURACY. Inspection of the differential equations derived for the first two birefringence procedures indicates that the general method is potentially superior to the optic angle method. Presence of the 2cotVdV term in the latter decreases the relative accuracy markedly. Total birefringence may be more accurately determined therefore on an optic normal section using the general method.

It is probable that the fractional deviations in the Emmons extrapolation method are of the same order of magnitude as those in the optic angle method, i.e., somewhat less accuracy is to be expected than in the general method.

Comparison of the general method (indirect) with direct determinations of B may be made in an approximate way as follows. Where refractive indices are determined to ±.001 (immersion method) the uncertainty in birefringence would be ±.002. For $B = .01$ the fractional deviation is then 20%; for $B = .10$ it is 2%. Inspection of the range of values in Figs. 12 and 13 for the indirect general method indicates that a total fractional deviation in birefringence of 15% might commonly occur. By using thick sections and selecting grains which do not require appreciable rotation for their orientation, the above value might easily be reduced to 5% as a maximum expected error. Comparison of the two methods depends therefore on auxiliary data, particularly on the magnitude of B and θ. For low birefringence the indirect general method may, in many cases, be preferable; for high birefringence the direct method is superior. Values of B obtained from precise prism determination of refractive indices would, of course, be superior in all cases to the indirect method.

DETERMINATION OF OPTIC ANGLE

Accurate information regarding the size of the optic angle in biaxial crystals is less important than accurate determination of refractive indices. However, as a number of procedures for optic angle determination are in common use, it is advisable to consider their relative merits.

COMPENSATOR METHOD. The approximate relation between optic angle and birefringence, $\sin^2 V = B_P/B_T$ is equivalent to $\sin^2 V = \Gamma_P/\Gamma_T$, where retardations are computed for a common thickness of section, Γ_P is the retardation in a section normal to X or Z, and Γ_T is the retardation in a section normal to Y. Wright's graphical solution of this equation is given by Emmons (1943, plate 11). Differentiating,[11]

$$dV = \frac{\Gamma_T d\Gamma_P - \Gamma_P d\Gamma_T}{\Gamma^2_T \sin 2V} \cdot$$

Using the Berek compensator, $d\Gamma_P$ and $d\Gamma_T$ are obtained from Fig. 12. In Fig. 14 dV/V (%) is plotted against Γ_T for several selected values of V. In general, accuracy is seen to be greatest for large retardations; in particular, where V is large as well.

As the basic formula above is an approximation, an appreciable correction to V must be applied where $B > 0.1$ (Larsen and Berman, 1934, Fig. 1). This correction, however, would result in negligible change in Fig. 14.

REFRACTIVE INDEX METHOD. The approximate equations $\cos^2 V_\alpha = (\beta\text{-}\alpha)/(\gamma\text{-}\alpha) = \sin^2 V_\gamma$, and $\sin^2 V_\alpha = (\gamma\text{-}\beta)/(\gamma\text{-}\alpha) = \cos^2 V_\gamma$ may be used to determine V if all three indices are known. The subscript α refers to a negative, γ to a positive mineral. Differentiating $\cos^2 V_\alpha$,

---

[11] The negative sign in the expression is changed to positive for computation of maximum error.

$$dV = \frac{(\gamma - \alpha)d\beta + (\beta - \gamma)d\alpha + (\alpha - \beta)d\gamma}{(\gamma - \alpha)^2 \sin 2V}.$$

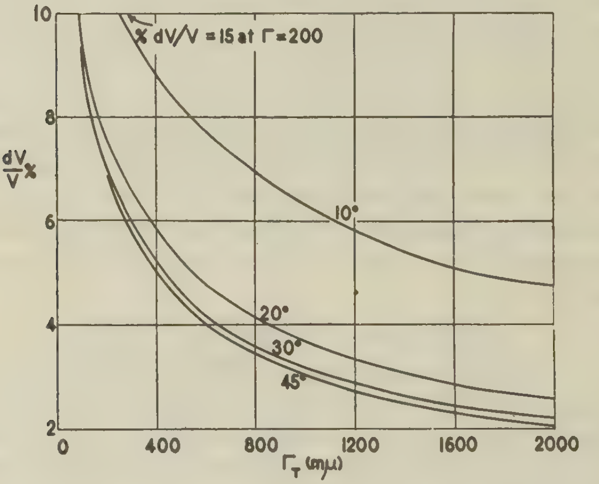

FIG. 14. *Compensator method.* Variation in accuracy of V for different values of total retardation (Γ_T). Diagram shows curves for four values of V.

As $\alpha < \beta < \gamma$, dV will have its maximum value where $d\beta$ is positive, $d\alpha$ and $d\gamma$ are negative. The equation is then rewritten

$$dV = \frac{(\gamma - \alpha)d\beta - (\beta - \gamma)d\alpha - (\alpha - \beta)d\gamma}{(\gamma - \alpha)^2 \sin 2V}.$$

Furthermore, $d\alpha = d\beta = d\gamma$, permitting the substitution of dn, so that

$$dV \text{ (radians)} = \frac{2dn}{(\gamma - \alpha)^2 \sin 2V} \quad \text{or} \quad dV \text{ (degrees)} = \frac{57.3 \times 2dn}{(\gamma - \alpha)^2 \sin 2V}$$

The uncertainty in n for the immersion method need not exceed ±.001, and for precise prism work ±.0001. Figure 15 is constructed for these values of dn, the curves representing various values of V as marked. In general, accuracy is greatest for high birefringence; in particular for high V values. It is obvious that an optic angle computation where dn = .001 is useful for relatively few substances (see Mertie, 1942), and that prism refractometry is required if any precision in V is expected by this method. Even with precision methods the accuracy is low if V is small.

EXTINCTION ANGLE METHOD. This method, first made practical by Berek (1924) and later amplified by Dodge (1934), provides a means of determining the optic angle independently of either refractive indices or retardation. It is discussed in two parts as outlined below.

Optic plane horizontal. This is the most useful case. The geometrical relations are as follows (Dodge, 1934):

$$\phi = \frac{K + K'}{2}, \quad \tan K = \tan(\bar{\phi} + V)\cos x, \quad \tan K' = \tan(\bar{\phi} - V)\cos x,$$

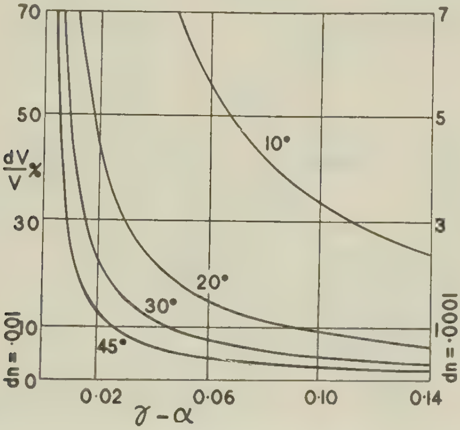

FIG. 15. *Refractive index method.* Variation in accuracy of V for different values of total birefringence ($\gamma - \alpha$). Curves shown for optic angle values of 10°, 20°, 30°, 45°. Based on refractive index uncertainties of .001 and .0001.

where the following rotations are made, in the order listed—

$\bar{\phi}$ is a fixed angle of rotation on the outer vertical axis of the stage;
x is a fixed angle of rotation on the outer east-west axis of the stage;
ϕ is an angle of rotation to extinction made on the microscope axis.

The graphical solution of these equations will be found in Dodge (1934) and also in Emmons (1943).

For the so-called "normal" case, where $\bar{\phi} = 45°$, and x is set equal to some given angle, we assume V and ϕ to be the only variables[12] in the above relation. Differentiating,

$$dV = \frac{2d\phi}{\sin 4\phi \tan 2V}.$$

---

[12] The uncertainty in x arising from incorrect orientation of the optic symmetry plane is lessened very considerably here by the large $\bar{\phi}$ value used, and is neglected in the differential equation. Where $\bar{\phi}$ is small x cannot be considered constant.

Fig. 16, showing dV/V plotted against V, contains two curves (full lines) derived from this equation, for values of $x=54.7°$ and 70°. The uncertainty in ϕ need not exceed ±1° if the optic axes are more nearly horizontal than vertical for the orientation in which ϕ is determined. If, however, the opposite condition holds, as it will in many cases, the uncertainty in ϕ is likely to be more nearly ±2°. As Fig. 16 is based on this larger value, dV/V may be halved if the optic axes approximate a horizontal position under the conditions just stated. It is seen that high V and high x increase the potential accuracy of the measurement. Two incomplete curves for $\bar{\phi}=15°$ and 30° (both for $x=70°$) have also been plotted, using the slopes of the proper curves given by Dodge (1934, plates I and II). Although these curves indicate higher accuracy than where $\bar{\phi}=45°$, it must be recalled that x is not constant for such small values of $\bar{\phi}$ (see footnote to previous paragraph). As the differential equation for $\bar{\phi}<45°$ and x variable is extremely cumbersome, no computations have been made. However, the discrepancy in fractional deviation between curves based on $\bar{\phi}=45°$ and $\bar{\phi}=15°$ is less than Fig. 16 indicates.

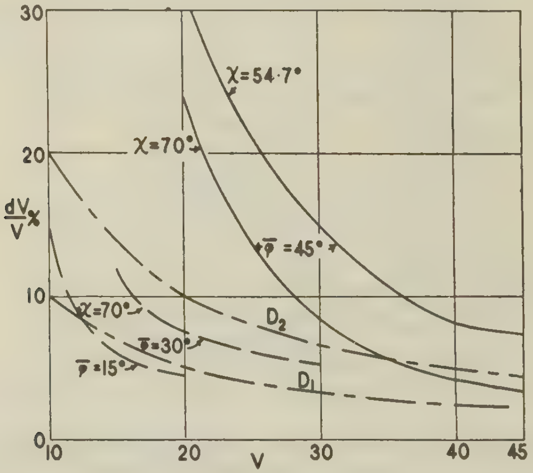

FIG. 16. *Extinction angle method* (*optic plane horizontal*). Variation in accuracy of V for different values of V. Full lines for $\bar{\phi}=45°$ and $x=54.7$ and 70° as marked. Broken lines for $x=70°$ and $\bar{\phi}=15°$ and 30°. These four curves based on an uncertainty in ϕ of ±2°. Curves D_1 and D_2, for direct readings of optic angle, are based on uncertainties in the optic angle of 1° and 2°, respectively.

Figure 16 includes also two curves, marked D_1 and D_2, which show the variation in accuracy where V is measured directly. D_1 is based on the case where both optic axes are measured and the uncertainty may attain a value of ±1°; D_2 is for the case of one measured axis and an uncertainty of ±2°. Assuming an uncertainty of 2° in ϕ, and $\bar{\phi} = 45°$, it is seen that the computed values of V approximate the accuracy of the direct method only for the highest values of V; for small optic angles a small value of $\bar{\phi}$ is required to attain comparable accuracy.

Optic Plane Vertical. This orientation is considered here only for the case of a horizontal acute bisectrix. Where the acute bisectrix is vertical it is usually possible to measure both axes directly and thus avoid indirect methods. The basic equation (Dodge, 1934) is:

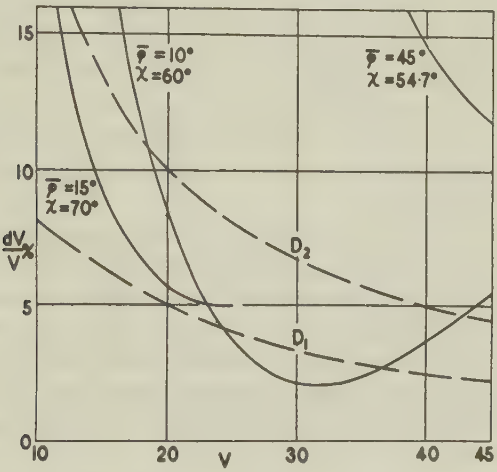

FIG. 17. *Extinction angle method* (*optic plane vertical*). Similar to Fig. 16.

$$\sec V = \left(\sin^2 \bar{\phi} + \frac{\cos 2\bar{\phi}}{\sin^2 x} - \frac{\cos x}{\sin^2 x} \sin 2\bar{\phi} \cot 2\phi\right)^{1/2}$$

where $\bar{\phi}$, x, and ϕ are the same quantities used in the previous section and rotations are made in the same order. As before, ϕ and V are assumed to be the only variables, although this is true only where x is not appreciably affected by incorrect setting of the optic symmetry plane. Differentiating,

$$dV = -\frac{\cos x \sin 2\bar{\phi} \cos V d\phi}{\sin^2 x \sin^2 2\phi \tan V \left(\sin^2 \bar{\phi} + \frac{\cos 2\bar{\phi}}{\sin^2 x} - \frac{\cos x}{\sin^2 x} \sin 2\bar{\phi} \cot 2\phi\right)^{1/2}}.$$

For selected values of $\bar{\phi}$ and x this expression becomes much less formidable in appearance. The uncertainty in ϕ is taken as ±2°, but with the same reservation as discussed in the previous section. Figure 17 shows the variation in dV/V (%) with change in V for two typical curves taken from Dodge (1934, plates IV and V). In addition, a portion of the fractional deviation curve for the "normal" case is included (upper right of Fig. 17). Where the uncertainties in ϕ are the same it is seen that greater accuracy can be obtained in the computation of V with small $\bar{\phi}$ than is otherwise the case.[13] The curves D_1 and D_2 described in Fig. 16 are replotted in Fig. 17 for comparison of direct and computed values of V. As they cover about the same field in the diagram as the two curves $\bar{\phi}=10°$ and $\bar{\phi}=15°$, it is seen that there is little to choose between the two methods under these conditions. If, however, the orientation conditions indicate a lower value of $d\phi$ than that on which Fig. 17 is based, the computed value may be more accurate than that obtained by direct measurement. In all cases, direct measurement is preferable to the computed value based on $\bar{\phi}=45°$.

Interference figure methods. A number of methods based on interference figures are known (Johannsen 1918), but few are in widespread use at present. Where $2V<60°$ and a centered acute bisectrix figure is obtainable, Mallard's method is convenient to use. The basic relation is $\sin V = D/K\beta$, where D = one-half the distance between the points of emergence of the optic axes of the crystal plate, K = a constant of the optical system (previously determined using minerals of known optic angle), β = intermediate refractive index of the crystal under examination.

Assuming any random error in K to be negligible relative to the uncertainty in measuring 2D, differentiation of the above equation gives

$$dV \text{ (radians)} = \tan V\left(\frac{dD}{D} - \frac{d\beta}{\beta}\right).$$

If K = 30 for the given optical system the uncertainty in 2D need not exceed 0.5 scale divisions, so that dD = .25. If $d\beta$ is known to ±.001, it is easily shown that $d\beta/\beta$ is negligible relative to dD/D, so that, finally, dV (degrees) = 57.3dD/D tan V. Curve M in Fig. 18 is based on this equation. It is seen that the accuracy of the method is low for small optic angles.

Curve C shows the variation of dV/V with V where the optic angle is estimated from curvature of a single isogyre. With practice the uncertainty in estimating 2V by this method[14] need not exceed 6°, so that dV = 3°. Curve C is based on this value.

---

[13] The same comment made in the previous section regarding uncertainty in x for low $\bar{\phi}$ values applies here.

[14] E. S. Larsen, personal communication.

For comparison, curve D_1 (showing the fractional deviation in the direct method for $dV=1°$) is included in Fig. 18.

COMPARATIVE ACCURACY. Inspection of the diagrams (Figs. 14–18) makes apparent the difficulty of general comparison of optic angle methods. Except where V and B are small, the refractive index method is undoubtedly the most accurate if the indices are determined by the minimum deviation prism method. However, where the indices are determined by matching with an oil to ±.001, the method yields results which are not much better on the average than results obtained from estimating the curvature of an isogyre.

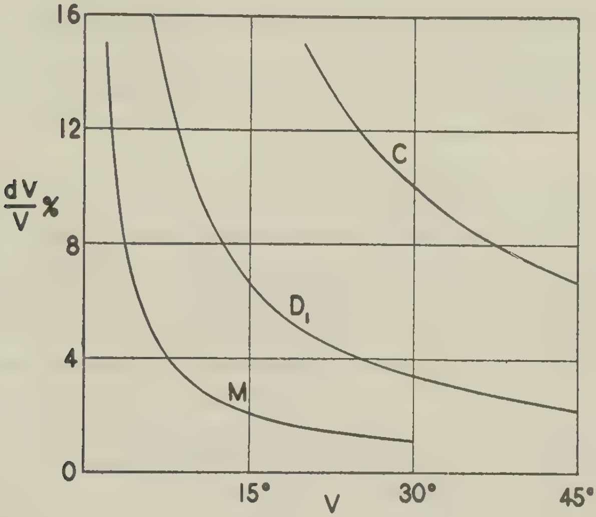

FIG. 18. *Interference figure methods*. Variation in accuracy of V for Mallard's method (curve M), where $K=30$ and $dD=.25$. Curve C represents the estimation method where $dV=3°$. Curve D_1 is for the direct method where $dV=1°$.

Where favorable conditions for rotation exist, and with the uncertainty in ϕ not in excess of 1°, the extinction angle method will give values of V almost as free from error as the refractive index method (for $dn=.0001$ and $B>.02$). Where the uncertainty is ±2°, however, the accuracy is approximately the same as the refractive index method with $dn=.001$.

Comparison of the compensator method with other methods requires the assumption of a definite thickness for the section. Thus for $t=.02$ mm. the dV/V compensator values are about intermediate between those obtained from the extinction angle and refractive index methods.

Although of restricted application, Mallard's interference figure method is more accurate than direct measurement of optic angle with the universal stage, if the maximum values for dD and dV used in the diagrams are accepted as probable.

Comparison of the three indirect universal stage methods with the direct method shows in most cases that the latter is at least equal, or definitely superior, in accuracy to the former. Exceptions occur with the refractive index method where $dn = .0001$ and B and V are moderate to large, and with the extinction angle method where ϕ is small and x large.

For all methods less accuracy is possible for low values of optic angle than for high values.

SUMMARY

The usefulness of the diagrams presented in this paper depends on good judgment in selecting a reasonable maximum value of the uncertainty in any given measurement. In choosing the values on which the preceding figures are based the authors have assumed a skilled operator who has at his disposal good material and equipment. Where a series of readings of the same measurement is taken and a "probable error" computed, greater accuracy should be attained than shown here. Where the working material is poor less accuracy is to be expected. In general, where the uncertainties in measurement are believed to differ from those used in the diagrams, it is necessary only to substitute in the differential equation the revised value for the original and to construct a new graph.

A set of these graphs readily available in the laboratory should prove highly useful by providing instant information regarding the order of magnitude of the maximum error to be expected in a given procedure. It is the authors' hope that in time a more realistic attitude will be developed toward mineralogic measurements than is now apparent from much of the published quantitative data.

ACKNOWLEDGMENTS

The writers are indebted to Dr. E. S. Larsen of Harvard University for critical examination of the manuscript and for several helpful suggestions.

REFERENCES

BANNISTER, F. A., AND HEY, M. H. (1937), A new micro-pyknometric method etc.: *Mineral. Mag.*, **25**, 30–37.

BEREK, M. (1913), Zur Messung der Doppelbrechung etc.: *Central. Miner.*, 388–396.

BEREK, M. (1924), *Mikroskopische Mineralbestimmung* etc.: Gebrüder Borntraeger, *Berlin.*

BERMAN, HARRY (1939), A torsion microbalance for the determination of specific gravities of minerals: *Am. Mineral.*, **24**, 434–440.

BUERGER, M. J. (1942), *X-ray Crystallography:* John Wiley and Sons, Inc., *New York.*

Dodge, T. A. (1934), The determination of optic angle etc.: *Am. Mineral.*, **19**, 62–75.

Ellsworth, H. V. (1928), A simple and accurate constant-volume pyknometer for specific gravity determinations: *Mineral. Mag.*, **21**, 431-435.

Emmons, R. C. (1943), The Universal Stage: *Geol. Soc. Am.*, *Memoir* **8.**

Gibb, T. R. P. (1942), *Optical Methods of Chemical Analysis:* McGraw-Hill Book Co. Inc., *New York.*

Gifford, J. W. (1902), Refractive indices of fluorite, etc.: *Proc. Roy. Soc.* (Lond.), **70**, 329–332.

Guild, J. (1923), Goniometry: *Dict. App. Physics*, **4**, 112, MacMillan & Company, Ltd., *London.*

Hey, M. H. (1933), On the accuracy of mineralogic measurements: *Mineral. Mag.*, **23**, 495–500.

Jahns, R. H. (1939), Clerici solution for specific gravity determination etc.: *Am. Mineral.* **24**, 116–122.

Johannsen, A. (1918), *Manual of Petrographic Methods:* McGraw-Hill Book Co., Inc., *New York.*

Ksanda, C. J., and Merwin, H. E. (1939), Improved technique in micropycnometric density determination: *Am. Mineral.*, **24**, 482–484.

Larsen, E. S., and Berman, Harry (1934), The Microscopic Determination of the Nonopaque Minerals: *U. S. Geol. Surv.*, *Bull.* **848.**

Mertie, J. B. (1942), Nomograms of optic angle formulae: *Am. Mineral.*, **27**, 538–551.

Tilton, L. W. (1935), Standard conditions for precise prism refractometry: *Jour. Res. Nat. Bur. Standards*, **14**, 393–418.

Tilton, L. W. (1942), Testing of Abbé refractometers: *Jour. Opt. Soc. Am.*, **32**, 371–381.

Timmermans, Jean (1912), Recherches experimentales sur la densité des liquides etc.: *Sci. Proc. Royal Dublin Soc.*, **13** (n.s.), 310–374.

Winchell, Horace (1938), A new micropycnometer for the determination of densities of heavy solids: *Am. Mineral.*, **23**, 805–810.

DIAGNOSTIC CRITERIA FOR CLAY MINERALS*

W. F. Bradley, *State Geological Survey, Urbana, Illinois.*

Abstract

The value of the utilization of complex formation between clay minerals and suitable types of organic liquids in the identification and characterization of clay minerals is illustrated by means of a series of such complexes between ethylene glycol and various clay minerals. Particular attention is devoted to mixed layer minerals involving intergrowth of montmorillonite with illite.

Recent observations on molecular associations between organic liquids and the montmorillonite type of clay minerals (1) have suggested that similar associations may be used to classify the other clay minerals. Not only is it true that many organic materials are available which associate with montmorillonites in a clearly characteristic manner, but there is an extensive list of incompletely characterized clays in which low-temperature water seems sufficiently important that one might anticipate similar associations.

For the limited number of observations reported here, the following thoughts have guided the choice of illustrative examples. The associations of poly oxygen compounds with montmorillonite are assumed without the complicating factor of base exchange, and of these, the complex that contains ethylene glycol, the simplest molecule, invariably gave an excellent clearly characteristic *x*-ray diffraction diagram. Ethylene glycol is both small enough to minimize possibilities of steric hindrance and sufficiently non-volatile to keep clay specimens damp during the registration of diffraction patterns, even though no complex may have been formed.

The Montmorillonite Group

Associations of montmorillonites with organic materials have been studied from time to time (2, 3, 4, 5) and have been the basis of Hendricks and Alexander's color reaction for the group (6). *X*-ray diffraction diagrams represent only one of the methods by which montmorillonites are habitually recognized. Justification for the further complication of utilizing *x*-ray diffraction from chemically treated preparations must come from the characteristically more clean-cut appearance of patterns. Natural minerals of the montmorillonite group afford diffraction patterns which vary enormously in the relative prominence of the basal reflections (commonly used as the diagnostic criterion) and of the prismatic reflections, to say nothing of the variations in diffraction angle for the first order of the base, and the vast differences in the perfection of development of succeeding orders. Montmorillonites soaked in glycol and drained dry before registration of the diffraction diagram have invariably afforded a clear sequence of higher orders of diffraction from the base, of greater intensity relative to prismatic reflections than are observed for natural materials, and representing a c-axis length not appreciably affected by previous history or humidity. This configuration has been interpreted to represent individual montmorillonite layers interleaved with double layers of glycol molecules, comprising a periodicity along c^* of

---

* Published with the permission of the Chief, Illinois State Geological Survey.

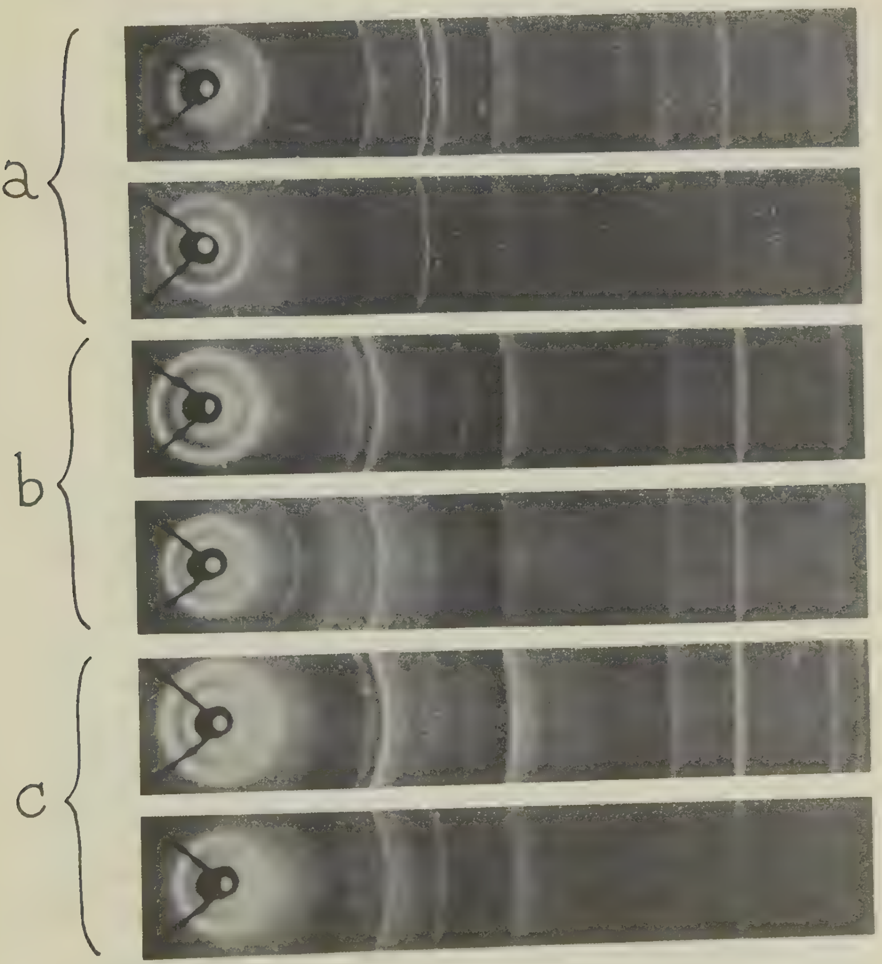

FIG. 1. *X*-ray powder diffraction diagrams of natural montmorillonites compared with the diagrams after glycol treatment. (a) Wyoming bentonite; (b) pink montmorillonite from Tatatila, Vera Cruz, Mexico, U. S. Nat. Mus. no. 101836; (c) montmorillonite from Rodeout, Utah. Natural clay above, and treated material below for each.

17 Å. Diagrams have looked about equally clear for glycol complexes prepared from natural materials for which, when untreated, the higher orders of the base were: (a) clear and related to a 12.5 Å periodicity; (b) clear and related to a 15 Å periodicity; or (c) poorly defined or missing. Illustrative examples are shown in Fig. 1. In cases where montmorillonite is only a minor component in the presence of other material, diffraction effects from the complex are also more easily discerned than are those of the untreated material.

The Kaolinite Group

The kaolinite group of minerals, kaolinite, nacrite, and dickite, include no molecular water in their crystallizations, and exhibit no reactions with liquids which can be followed by diffraction methods. It is undoubtedly true that there is strong adsorption of organic liquids on the crystallite surfaces, as shown in the properties of materials like plasticene (or modelling clay), but the actual crystallization (and diffraction patterns) are unaltered.

Endellite and Halloysite

An unfortunately confused state of nomenclature with regard to halloysite has recently been resolved by the proposal of "endellite" as a name for the hydrated member (7).

Both minerals are recognized readily enough on the basis of their normal diffraction diagrams, but their behavior toward the organic liquids is interesting. The displacement of molecular water from endellite by ethylene glycol (and by other solvents) both serves to confirm its structure and is an unmistakable criterion of identity.

The characteristic strong diffraction line of endellite at 10.1 Å is displaced to 10.8 Å in the ethylene glycol complex. First, third, and fifth orders from this spacing, which is the complex thickness, are apparent in each case. These thicknesses represent the thickness of a kaolinite layer plus, respectively, one water layer of about 3.0 Å and one glycol layer of about 3.6 Å. In contrast with the montmorillonite complexes, which have two layers of glycol, it is pointed out that endellite has only one oxygen surface and montmorillonite has two oxygen surfaces available. It is assumed that the stability of each configuration is governed by the attraction of the oxygen surfaces for the slightly active methylene groups.

The dependence of the mean refractive index of endellite on the constitution of the index oils was noted by Correns and Mehmel (8) but was questioned by Faust et al. (7). It is clear that the indices of complexes of the sort here described must differ appreciably from those of the natural mineral. The calculated mean index for endellite is 1.49, and an estimated index for the glycol complex, based on the molecular volume of liquid glycol is 1.52, probably ±0.01. The observed index for the complex is 1.525, determined by rapid comparison with liquids made up from mineral oil and monochloronaphthalene. The endellite for this preparation was selected from material from Eureka, Utah, and did not contain more than 5 or 10 per cent of halloysite. Complexes of endellite with

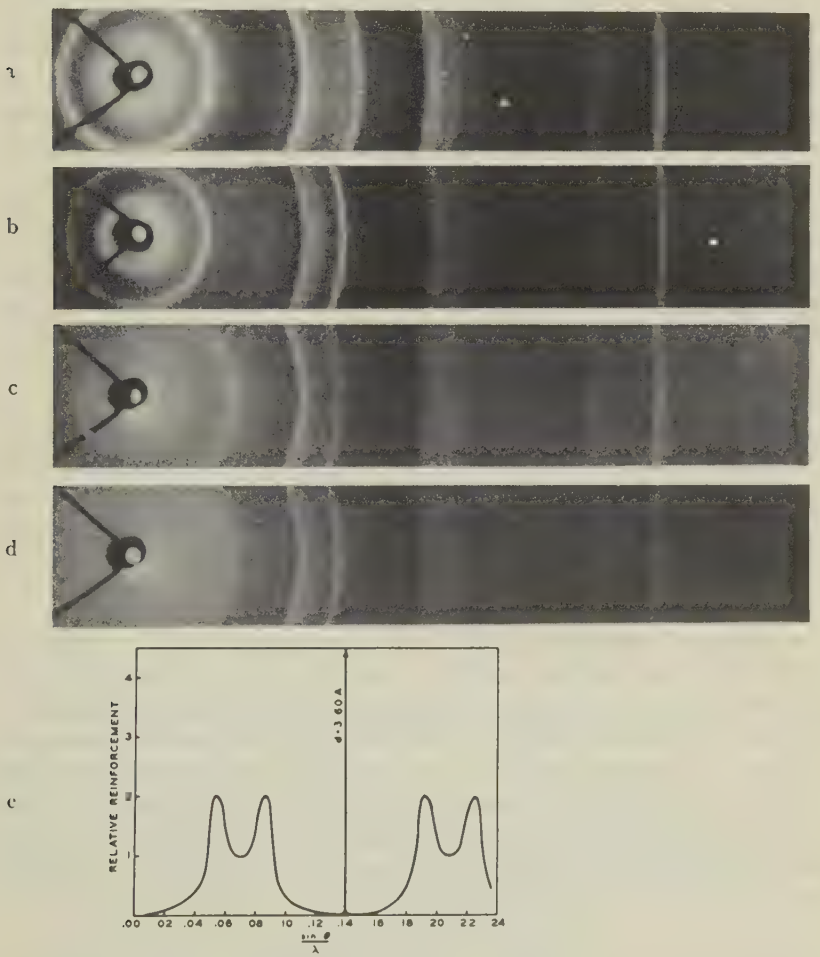

FIG. 2. The association of ethylene glycol with halloysite. (a) natural endellite; (b) endellite treated with ethylene glycol; (c) halloysite resulting from aging of (a); (d) halloysite treated with ethylene glycol; and (e) a plot of Hendricks and Teller's function for units of 10.8 and 7.2 Å, plotted to the approximate scale of the diffraction diagrams. The arrow indicates the position of normal reflection.

other active liquids (1) would also have indices ranging from 1.52 to 1.55.

Halloysite derives from endellite upon loss of the molecular water. The resultant material is very porous, retains its original bulk, and readily absorbs water, but the structural change from the endellite crystallization to a kaolinitic crystallization is irreversible, or at best incompletely reversible. Wet halloysite specimens give essentially the halloysite diffraction diagram.

The diffraction diagram of halloysite wet with ethylene glycol differs in a distinctive way from those of endellite, halloysite, or kaolinite. The prismatic interferences of endellite and halloysite are unchanged, but of the possible interferences related to the base, only one line, at 3.6 Å, appears sharp and well-defined. In the region corresponding to periodicities from about 11 to about 7 Å, there appears only a broad weak band, in which the intensity seems to be somewhat higher near its edges.

The function derived by Hendricks and Teller (9) for mixed layer minerals applies only to equally probable units of the same form factor. In the absence of suitable information about the form factors it is impractical to attempt to compute a theoretical intensity distribution for this case (as will later be done for a more apt example), but a comparison of the plot of Hendricks and Teller's function with the diffraction diagram in Fig. 2 indicates clearly that a random or near random interleaving of 10.8 and 7.2 Å units would produce the same sort of diagram as is observed. Actually, it seems indicated that simple 7.2 Å units outnumber the complex 10.8 Å units, but the characterization of halloysite as the collapsed structure subject to random penetration of active liquids, seems justified.

ILLITE

Although illites invariably contain more or less molecular water, as is apparent from thermal analysis curves (10), the crystallization is determined by mica principles, and the position in the structure of any water not merely absorbed on exterior surfaces is not known. Treatments of illite with organic liquids do not therefore result in any structural changes, and diffraction diagrams do not differ from those of the untreated materials. The frequently encountered instances in which illites are observed to be mixed with extraneous layers are discussed in connection with the mixed layer minerals.

MIXED LAYER MINERALS

Several instances have been reported (11, 12, 13, 14, 15) in which it seemed that a specimen under consideration was actually composed of irregularly alternating layers of two distinct minerals. The treatment of diffraction effects from such mixed layers by Hendricks and Teller (9) has afforded a basis on which one can hope to examine in detail some of these suspected instances.

A particularly fortunate case has been that of some bravaisite from the type locality, U. S. Nat. Museum Specimen No. 4918.* A study has shown not only that this material is about equally divided between two species, but also that the two form factors are similar enough to permit a reasonably accurate construction of the calculated diffraction effects.

Grim and Rowland (10) concluded from thermal analysis curves that this material included both illite and montmorillonite. If it be assumed, then, that this material be made up of a random stacking of equally probable illite and montmorillonite layers, one case can be developed for the natural material itself, and a second case can be developed for the mixture of illite with glycol-complexed montmorillonite which would result from glycol treatment.

In connection with the previous study of complexes of montmorillonite with various types of organic liquids (1), observed 00*l* diffraction sequences from a series of complexes of varying cell heights have been available. Estimated intensities for the powder diffraction rings for this entire group have been plotted together against sin θ/λ, and Fig. 3 is a smooth average curve summarizing the composite data. Although each individual diagram has been rather strongly influenced by the organic matter, the allowable degree of error for the present purposes is so great that this curve adequately represents not only the contribution of the montmorillonite layers, but also the contribution of the similarly constituted, but rigid, illite layers.

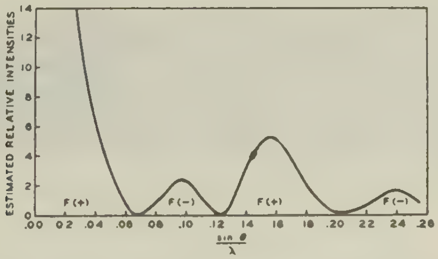

FIG. 3. Compositite curve of estimated relative intensities of 00*l* powder diffraction rings versus sin θ/λ taken from a group of organic molecule-montmorillonite complexes of various *c*-axis periodicities.

To arrive at the angular distribution of scattered radiation from the random mixed layer sequences assumed, then, it is only necessary to multiply the ordinates of Hendricks and Teller's function for each case by the ordinates of Fig. 3. In Fig. 4 curves derived in this way for a mixture of 10 Å and 15 Å units, and of 10 Å and 17 Å units are compared with the diffraction diagrams of bravaisite and of glycol treated bravais-

---

* Furnished through the courtesy of Dr. W. F. Foshag.

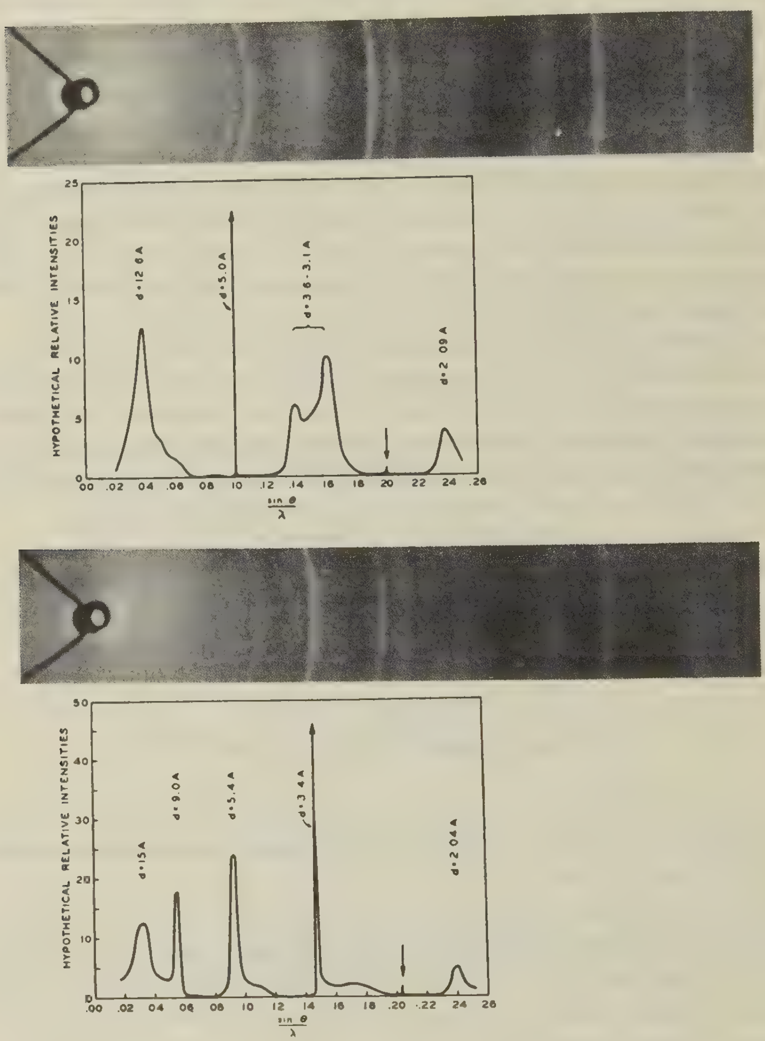

Fig. 4. Bravaisite, Noyant Allier, France, U. S. Nat. Mus. no. 4918 (above) and the same treated with ethylene glycol (below), each compared with its synthesized curve for random mixed layers to scale approximately equivalent to the diffraction diagram. Erect arrows indicate positions of normal or near normal reflection. Inverted arrows indicate normal reinforcements in the mixing function which are extinguished by the form factor.

ite, respectively. Reasonable agreement in the position, relative intensity, and apparent breadth of all the important maxima is evident.

No other instance has been encountered in which the relative frequencies of illite and montmorillonite layers are nearly enough equal to conform to Hendricks and Teller's equation. However, the principle can probably be extended in a qualitative way to cases in which one species predominates over the other to a moderate extent. If for example, illite occurred more frequently than montmorillonite, we would expect from inspection of the function that in general maxima would approach the position of the sharp interference maxima of illite. For the natural material, where the form factor extinguishes one of the small-angle maxima of the complex function, the diagram would only more nearly resemble illite. For glycol-treated material, however, both of the small-angle maxima should persist and should merely approach each other.

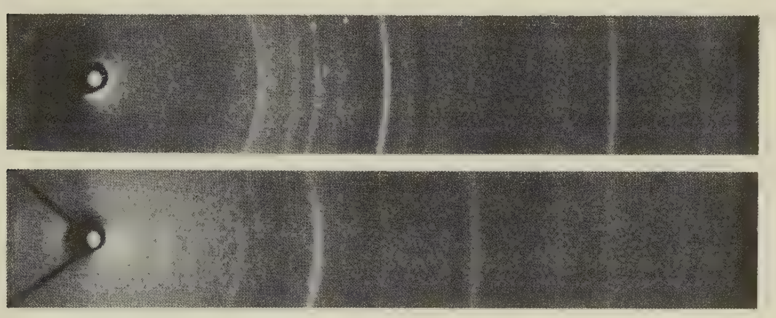

FIG. 5. Powder diffraction diagram of "glimmerton," Sarospatak, Hungary, from U. Hofmann, treated with ethylene glycol (above), compared with illite purified from shale from Alexander County, Illinois, after the same treatment (below).

Among the natural materials in which two small-angle maxima are developed by glycol treatment are several which have heretofore been described as illites or at least as mica-like clays. These include the "glimmerton" from Sarospatak, Hungary (16), the illite purified from an underclay in Grundy County, Illinois (17), a "metabentonite" from High Bridge, Kentucky (10), and possibly some glauconites. In Fig. 5 the diagram for glycol-treated "glimmerton" is reproduced. For specimens with lesser proportion of montmorillonite layers the diagrams are less clear. The ratio of mica to montmorillonite layers in the "glimmerton" is probably near 2; in the other cases, somewhat higher. A diagram of a glycol-treated illite, unmixed with extraneous layers, is included for comparison.

Mixed layer minerals of other types also no doubt exist, of which particularly a mixture of montmorillonite and illite with montmorillonite predominating should be amenable to interpretation by this method, but no clear cut occurrence has yet been recognized.

Miscellaneous Minerals

The number of hydrous clayey or clay-like minerals which have been described and named is too great to attempt to catalogue them here. Probably the greatest number of these are the varieties which are actually members of the montmorillonite group. Most of the specimens of this sort reported on by Grim and Rowland (10) have been made available for examination in this study. The characteristic 17 Å glycol complex is readily prepared from all of the so-called beidellites discussed by them, except their number 8 Å (U. S. Nat. Museum no. R7595), from the nontronites, the white Hector magnesium clay, smectite, chloropal, and volkonskoite.

Loosely related to these materials are two other mineral types in which comparable structural units appear, the vermiculites and attapulgite.

Vermiculites.—Although the ideal structure of vermiculite (12) immediately suggests that the interlayer water could be displaced by organic liquids, no attempts to make such complexes from the familiar crystalline materials have yet been successful. However, a series of cryptocrystalline weathered amygdules collected by Dr. R. M. Grogan from basic Keweenawan flows along the north shore of Lake Superior, which have been identified as vermiculites by x-ray diffraction methods, do form the same sort of 17 Å glycol complex as is observed for montmorillonites. In view of the known tendency for vermiculites to occur mixed with chlorites, it seems quite possible that such mixing, particularly if it were lateral within layers, might inhibit the introduction of glycol into the natural large crystals even though it would be readily introduced into a fine-grained, or into an ideal specimen.

Attapulgite.—The association of any individual water molecule with the silicate portion of attapulgite is probably due to hydrogen bonding, analogous with that exhibited by the water associated with montmorillonite, but the disposition of the silicate chains (18) confines the water to narrow channels and precludes the changes in dimensions that are observed for swelling clays. The water channels have cross sections of about 3.7×6.0 Å, which might accommodate single strings of ethylene gycol, but in the absence of dimensional changes, only minor intensity variations are to be expected upon glycol treatment, and no obvious variations were noted in the diffraction diagrams. Refractive indices, however, are sharply reduced. Well-oriented flakes with $\gamma=1.540$,

$\gamma-\alpha=.032$, showed after treatment $\gamma=1.50$ with comparable birefringence. The calculated mean index for the silicate skeleton above is about 1.44. The observed indices can therefore apparently be considered to arise from extensive extraction of the hydrogen-bonded water accompanied by only very limited penetration of glycol into the channels.

SUMMARY

The association of certain organic liquids with clay minerals affords a basis for the classification of such minerals into the principal groups, and at the same time serves to confirm the general features of the respective structures.

ACKNOWLEDGMENT

The author is indebted to Dr. R. E. Grim who furnished many of the mineral specimens employed, and who determined the refractive indices that are cited.

REFERENCES

1. BRADLEY, W. F., *J.A.C.S.*, **67**, 975–981 (1945).
2. GIESEKING, J. E., *Soil Sci.*, **47**, 1–13 (1939).
3. HENDRICKS, S. B., *J. Phys. Chem.*, **45**, 65–81 (1941).
4. DAVIDSON, R. C., EWING, F. J., AND SHUTE, R. S., *Nat'l Pet. News*, **35**, No. 27, R318–321 (1943).
5. MACEWAN, D.M.C. *Nature*, **154**, 577–578 (1944).
6. HENDRICKS, S. B., AND ALEXANDER, L. T., *J. Am. Soc. Agron.*, **32**, 455–458 (1940).
7. ALEXANDER, L. T., FAUST, G. T., HENDRICKS, S. B., INSLEY H., AND MCMURDIE, H. F., *Am. Mineral.*, **28**, 1–18 (1943).
8. CORRENS, C. W., AND MEHMEL, M., *Zeits. Krist.*, **94**, 337 (1936).
9. HENDRICKS, S. B., AND TELLER, E., *J. Chem. Phys.*, **10**, 147–166 (1942).
10. GRIM, R. E., AND ROWLAND, R. A., *Am. Mineral.*, **27**, 746–761, 801–818 (1942).
11. GRUNER, J. W., *Am. Mineral.*, **19**, 557–575 (1934).
12. HENDRICKS, S. B., AND JEFFERSON, M. E., *Am. Mineral.*, **23**, 851–862 (1938).
13. GRUNER, J. W., *Am. Mineral.*, **29**, 422–430 (1944).
14. JACKSON, M. L., AND HELLMAN, N. N., *Proc. Soil Sci. Am.*, **6**, 133–145 (1941).
15. NAGELSCHMIDT, G., *Mineral. Mag.*, **27**, 59–61 (1944).
16. MAGDEFRAU, E., AND HOFMANN, U., *Zeits. Krist.*, **98**, 31–59 (1937).
17. GRIM, R. E., AND BRADLEY, W. F., *J. Am. Cer. Soc.*, **22**, 157–164 (1939).
18. BRADLEY, W. F., *Am. Mineral.*, **25**, 405–410 (1940).

ADDITIONAL OPTICAL AND CHEMICAL DATA ON THE STILPNOMELANE GROUP OF MINERALS

C. Osborne Hutton, *Geological Survey, Wellington, New Zealand.*

Summary

Since publication of a paper on the stilpnomelane group of minerals (Hutton, 1938), the author has succeeded in obtaining a member of this series with a composition considerably different from those previously analysed; in addition two analyses of stilpnomelanes have been published by other authors (Wager and Deer, 1939, p. 188; Ayres, 1940, p. 432), together with their optical constants. These analyses are discussed and the extent to which the provisional curves published earlier (Hutton, 1938, p. 187) require modification, is indicated.

Optical Data

The stilpnomelane newly analysed by Mr. F. T. Seelye for the writer was separated from an albite-epidote-stilpnomelane-chlorite schist containing minor amounts of quartz, titanite, muscovite, apatite, and calcite. The rock is coarsely crystalloblastic, strongly laminated, and schistose; it is a typical member of the green-schist facies as developed in the Chl. 4 subzone of the chlorite zone of western Otago (Hutton and Turner, 1936; Hutton, 1940). The stilpnomelane itself, in very coarsely crystalloblastic plates, and radiating or sheaf-like aggregates up to 5 mm. in length, is intimately interlaminated with plentiful chlorite from which it seems to be in the process of developing; it appears to lack any marked preferred orientation, and the sheaf-like aggregates in some cases lie transverse, in others parallel, to foliation and schistosity planes.

Optical properties of the associated chlorite are as follows:

$$\alpha=1.635\pm0.002$$
$$\beta=\gamma=1.640$$
$$\gamma-\alpha=0.005$$
$$2V=0°$$

Sign: negative
Elongation: positive
Pleochroism α = very pale greenish yellow to colourless.
Pleochroism $\beta=\gamma$ = deep grass green.
Absorption $\gamma=\beta>\alpha$
Dispersion $r>v$ (not strong).

These data indicate a composition just inside the field of brunsvigite in the sense used by Winchell (1936, p. 649, Fig. 4) in his most recent study of the chlorite group. In an earlier investigation of the chlorites occurring in schists of the chlorite zone of western Otago, the β values of over thirty chlorites were found to be within the limits 1.607–1.639 (Hutton, 1940, p. 19). The chlorite just described is thus a relatively iron-rich type.

The stilpnomelane mineral was separated from the schist by careful crushing, screening, and centrifuging methods following the procedure recommended previously (Hutton, 1938, p. 183). The analysis undertaken by Mr. F. T. Seelye is set out in Table 1A.

When α and γ for the three newly analysed stilpnomelanes (Table 1, A, B, C) are plotted against the ratio (Fe, Mg, Mn) O/ $(Fe, Al)_2O_3$ on the original diagram (Hutton, 1938, p. 187), the values given for the Otago mineral and that described by Ayres and Park (analyses A and B) agree reasonably well with the existing curves. In the case of the Greenland stilpnomelane (analysis C), however, the values for α and γ certainly fall close to the extension of these curves, as stated by Wager and Deer (1939, p. 190), but only if the composition is not taken into account. However, in the case of the Greenland stilpnomelane, the values of α and γ quoted indicate a (Fe, Mg, Mn) O/ $(Fe, Al)_2O_3$ ratio (molecular) of about 30/70, whereas the ratio calculated from the corresponding analysis is approximately 52/48. This discrepancy is possibly due to difference in composition between the unanalysed material used for refractive index determinations, and that selected by Wager and Deer for analysis. Furthermore, the relatively high CaO content of the analysis (4.28 per cent—a figure much higher than that in any other analysis available to the writer) points to possible impurity of the analysed material.

The writer now suggests a slight modification of the previously published curves to take into account the new data given in Table 1, A and B. This has been done in Fig. 1. Points for γ of the refractive index ellipsoid tend to lie along a straight line with no one point far removed from it, whereas with the exception of Nos. 2 and 11, none of the α values are far removed from the line representing α of the refractive index ellipsoid. For stilpnomelane minerals either β or γ can be determined with reasonable accuracy so long as thin, fully transparent platelets are used. Greater difficulty attends the determination of α owing to the micaceous habit of the mineral, and considerable care is required in order to obtain the minimum value. For the stilpnomelane mineral represented by analysis No. 4, the value for α is given by Gruner (1937, p. 914) as 1.58 ± 0.01; this limit of accuracy is unusually wide, so that the possible range has be indicated in Fig. 1.

CHEMICAL DATA

No further information of the chemical properties of members of the stilpnomelane group is available. However, Ayres' (1940, p. 433) statement that stilpnomelane from Crystal Falls was "not at all attacked by sulphuric" acid is surprising in view of the results of earlier experiments by the present writer (Hutton, 1938, p. 190). The newly analysed Otago

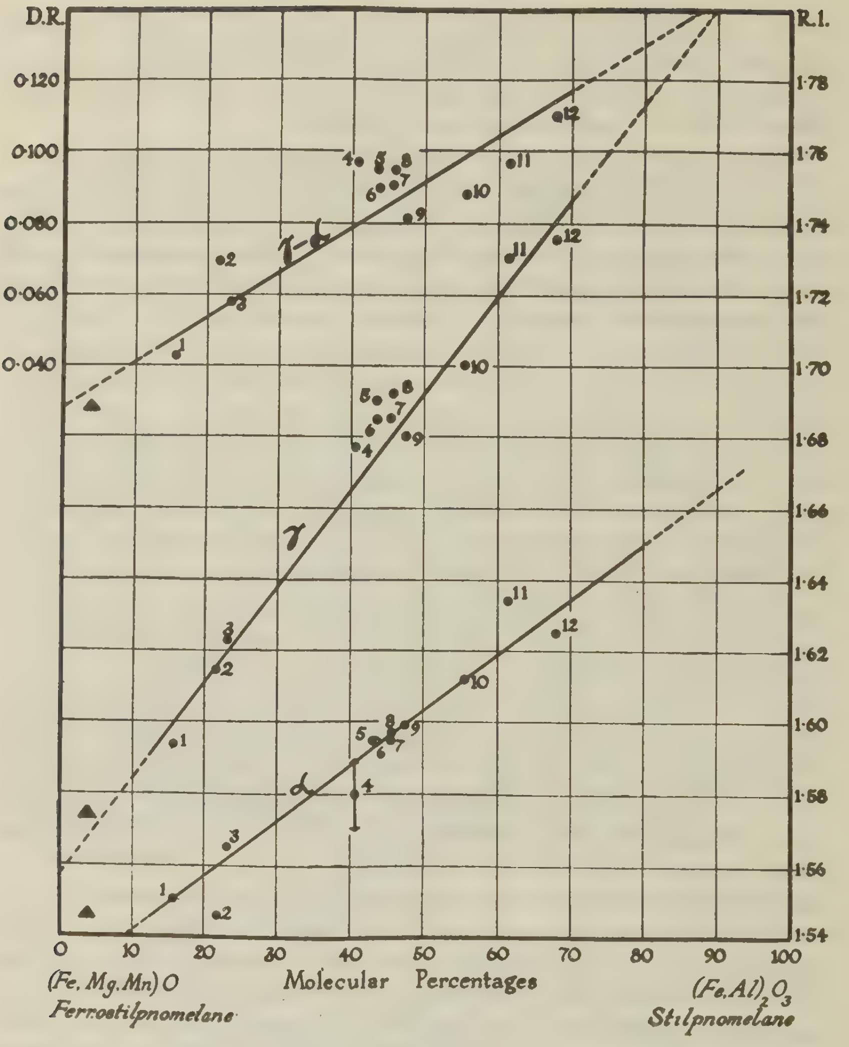

Key to Analyses in Fig. 1

Numbers in parentheses refer to the analyses plotted in Fig. 5 of Hutton (1938, p. 187).

1 (15). Western Otago. C. O. Hutton (1938, p. 184, anal. C, Table 3).
2 (1). Mesabi Range, Minnesota. F. F. Grout and G. A. Thiel (1924, p. 230, anal. No. 2).
3 (8). Theodor mine, Aumenau, Lahn. J. Holzner (1933, p. 216, anal. No. 4).
4 (12). Baern, Moravia. J. W. Gruner (1937, p. 913, anal. No. 4).
5. Western Otago. C. O. Hutton (1938, p. 184, anal. D, Table 3).
6 (4). Pen-y-rallt, Merionethshire. Hallimond (1924, p. 194, anal. No. 1).
7 (10). Zuckmantel, Austrian Silesia. C. O. Hutton (1938, p. 184, anal. E, Table 3).
8 (17). Anna Mine, Baern, Moravia. C. O. Hutton (1938, p. 184, anal. F, Table 3).

stilpnomelane (A in Table 1), when treated for 6 hours with 5N H_2SO_4 on the water-bath was completely decolourized, leaving colourless, isotropic plates of hydrated silica, with a refractive index of 1.438 after drying at 100°C. for 15 minutes.

TABLE 1. ANALYSES OF STILPNOMELANE

	A.	B.	C.
SiO_2	44.52	42.42	45.29
Al_2O_3	7.19	6.71	5.57
Fe_2O_3	27.32	33.24	23.95
FeO	3.31	0.85	8.99
TiO_2	0.10	—	0.02
MnO	0.42	2.27	1.14
MgO	5.63	5.20	3.30
CaO	0.23	—	4.28
Na_2O	0.32	—	nt.dt.
K_2O	1.77	—	nt.dt.
V_2O_3	nt.fd.	—	—
Cr_2O_3	nt.fd.	—	—
H_2O+	6.70	8.33	6.12
H_2O-	2.70	1.45	1.79
	100.21	100.47	100.45
$\alpha=$	1.612 ± 0.002	1.634	1.626
$\beta=\gamma=$	1.700	1.730	1.745
$\gamma-\alpha=$	0.083	0.096	0.119
2V	0°	0°	0°
Pleochroism:			
$\alpha=$	Bright golden yellow	As for β but weaker	Golden yellow
$\beta=\gamma=$	Very deep reddish brown	Golden yellow to chestnut brown	Dark reddish brown
Absorption	$\gamma=\beta>\alpha$	$\gamma=\beta>\alpha$	$\gamma=\beta>\alpha$
Sp. Gr.	2.82	—	—
$\frac{(Fe, Mg, Mn)O}{(Fe, Al)_2O_3}$	$\frac{44.47}{55.53}$	$\frac{38.70}{61.30}$	$\frac{51.88}{48.12}$

A. Stilpnomelane from albite-epidote-stilpnomelane-chlorite schist, p. 2264. Cowcliff Hill, Kawarau S.D. Analyst: F. T. Seelye.

B. Stilpnomelane from ferruginous Upper Huronian slates, Crystal Falls, Michigan. Analysts: V. L. Ayres and B. Park. The following elements were found spectrographically: Na, Li, Co, Ni, V, Ba, Zn. (V. L. Ayres, 1940).

C. Stilpnomelane from spherical vesicles in granophyre inclusion. Mellemö, Kangerdlugssuaq, E. Greenland. (L. R. Wager and W. A. Deer, 1939, pp. 188–189).

---

9 (9). Western Otago. C. O. Hutton (1938, p. 184, anal. B, Table 3).
10. Western Otago. Anal. A, Table 1, this paper.
11. Crystal Falls, Michigan. V. L. Ayres (1940, p. 432); or anal. B, Table 1, this paper.
12 (16). Western Otago. C. O. Hutton (1938, p. 184, anal. G, Table 3).
The solid triangles represent the plot of typical parsettensite (J. Jakob, 1923).

REFERENCES

AYRES, V. L. (1940), Mineral notes from the Michigan Iron Country: *Am. Mineral.*, **25**, No. 6, 432–434.

GROUT, F. F., AND THIEL, G. A. (1924), Notes on stilpnomelane: *Am. Mineral.*, **9**, 228–231.

GRUNER, J. W. (1937), Composition and structure of stilpnomelane: *Am. Mineral.*, **22**, 912–925.

HALLIMOND, A. F. (1924), On stilpnomelane in north Wales: *Mineral. Mag.*, **20**, 193–197.

HOLZNER, J. (1933), Beitrage zur Kenntnis der varistischen Gesteins- und Mineralprovinz in Lahn-Dillgebeit. 2. Über den Stilpnomelan von Grube Theodor (Lahngebeit) und einen beim Trennen mit Clericilosung auftretenden Basenaustausch: *Neues Jahrb. Min.*, Abt. A., Beil-Bd. **66**, 213–225.

HUTTON, C. O. (1938), The stilpnomelane group of minerals: *Mineral. Mag.*, **25**, No. 163, 172–206.

——— (1940), Metamorphism in the Lake Wakatipu region, western Otago, New Zealand: *D.S.I.R., Geol. Mem., No.* **5**.

HUTTON, C. O., AND TURNER, F. J. (1936), Metamorphic zones in north-west Otago: *Trans. Roy. Soc. N.Z.*, **65**, 405–406.

JAKOB, J. (1923), Vier Mangansilikate aus dem Val d'Err (Kt. Graubunden): *Schweiz. Min. Petr. Mitt*, **3**, 227–237.

WAGER, L. R., AND DEER, W. A. (1939), The petrology of the Skaergaard intrusion, Kangerdlugssuaq, East Greenland: *Meddel. om Grönland*, **105**, No. 4.

WINCHELL, A. N. (1936), A third study of chlorites: *Am. Mineral.*, **21**, No. 10, 642–651.

NOTES AND NEWS

PROBERTITE FROM LOS ANGELES COUNTY, CALIFORNIA

JOSEPH MURDOCH, *University of California at Los Angeles.*

A small specimen sent the writer recently, marked "Lang Borax Mine," proved on examination to be probertite. Since this mineral has been reported only from the Ryan and Kramer districts, in California, advantage was taken of a class field trip to the Lang area, where a good amount of the material was collected, and the occurrence confirmed. Identification was made by optical properties, the indices of refraction corresponding with those of probertite, and chemical tests confirmed these.

The appearance of the mineral is like that described by Foshag[1] for ulexite from this locality. The mineral occurs in lenticular aggregates of groups composed of slender radiating prisms up to 15×.5 mm. in dimensions, these groups themselves being more or less flattened. None of the specimens were found in place, as the material was all collected on the dump, but some with attached shale indicated their occurrence as lenticular nodules in a shale matrix.

This identity of appearance with Foshag's material, and with a similar occurrence of ulexite described from the Suckow mine in the Kramer district,[2] led to the thought that the determination might have been in error, and the mineral really ulexite. However, a careful re-check of the indices, and a determination of the water of crystallization confirmed its identity as probertite. Duplicate water determinations were run, giving values of 25.7% and 25.8% respectively, as compared with the theoretical value of 25.63%. All doubt was definitely cleared up by the discovery, among the specimens, of a few which were clearly different from the others, and were actually ulexite. This ulexite is essentially similar in appearance to the probertite, but is finer textured, much silkier in appearance, and lacking the definitely radial structure of the latter. Under the microscope it shows the normal ulexite indices, and the typical fine texture, and twinning. In further confirmation, two specimens were found showing the two minerals together, with ulexite covering the probertite rosettes, and enclosing residual patches of the latter mineral. The essential structure of the probertite groups was preserved, although not the detail. As a matter of fact, most of the material was unaltered probertite, with a very small number of the specimens showing any ulexite.

---

[1] Foshag, W. F., The origin of the colemanite deposits of California: *Econ. Geol.*, **16**, 204 (1921).

[2] Murdoch, J., Crystallography of ulexite: *Am. Mineral.*, **25**, 755 (1940).

Since the collection was made at random, this indicates the probable actual proportions of the two minerals in the deposit.

This relationship of ulexite and probertite induced the writer to look again at some specimens from the Kramer district, collected as ulexite. These were found to have been labelled "ulexite with residual kramerite," affording another instance of the same sequence. Foshag,[3] in writing of the Ryan District, suggested that ulexite had been altered to probertite although he did not find the two together anywhere. The basis for this idea was that the denser mineral (probertite) would be more likely to form from ulexite under the influence of pressure generated in the folding of the layers in this area. This does not appear to have been the case in the two cases which the writer has observed, since both at Lang and at Kramer the opposite sequence is clear.

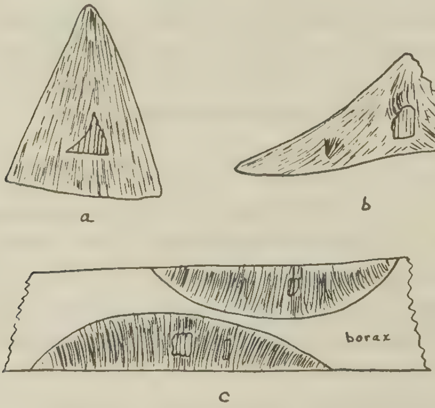

FIG. 1

At Kramer there are two examples of this relationship. First, the radiating groups or clusters of probertite described by Schaller[4] under the name kramerite, were found on one of the dumps by the writer as ulexite pseudomorphs, with occasional probertite cores. Second, specimens from the Suckow mine, just west of the other occurrence, show the curious fungus-like growths, and satiny cross-fiber veins mentioned from the kernite deposit,[5] in layers of clay and borax. Most of these are milky white, uniformly fine fibered ulexite, but some show residual patches of probertite, as noted casually at the time of collection. This can be identified easily by its glassier luster and coarser appearance, and some of the patches are large enough to provide material for optical determination. It was clearly the original mineral of these occurrences, but has been almost completely replaced. The colemanite produced by the further alteration of the ulexite, as observed by Schaller,[6] was not seen in any of the writer's material.

---

[3] Foshag, W. F., Probertite from Ryan, Inyo County, California: *Am. Mineral.*, **16,** 340 (1931).

[4] Schaller, W. T., Borate minerals from the Kramer District, Mohave Desert: *U.S.G.S. Prof. Paper* **158,** 139 (1930).

[5] Schaller, W. T., *op. cit.*, p. 139.

The relationship of probertite to ulexite in these specimens is illustrated by the accompanying drawings (Fig. 1), which represent the occurrence of the two minerals. There are three types of these, all from Kramer: (a) divergent, cone-shaped masses, usually in solid borax; (b) the fungus like forms, in layers of clay, or of clay and borax crystals; and (c) more or less hemispherical aggregates, occurring in narrow veins of secondary borax which cut the older ore.

The writer wishes to express his thanks to Mr. E. H. Peebles of San Gabriel, California, who sent in the specimen which led to the discovery of this new occurrence of probertite. Mr. M. Vonsen, of Petaluma, California, has informed the writer that he had recognized this material from Lang as probertite, some time ago.

[6] Schaller, W. T., *op. cit.*, p. 138.

Dr. Ralph E. Grim, petrographer and head of the Division of Petrography of the Illinois Geological Survey, has been made petrographer and principal geologist in charge of the Geological Resources Section. This section comprises the following divisions: coal, oil and gas, industrial minerals, clay resources and clay mineral technology, groundwater geology and geophysical exploration, areal and engineering geology, stratigraphy and paleontology, and subsurface geology. In the Geochemical Section of the Survey Dr. William F. Bradley has been made chemist and head of the Division of *X*-ray and Spectrography.

BOOK REVIEWS

THEORY OF *X*-RAY DIFFRACTION IN CRYSTALS by WILLIAM H. ZACHARIASEN, New York, John Wiley & Sons, (**1945**), V & 255 pages, 30 figures. Price $4.00.

This excellent book, written by one of the leading workers in the field, contains a complete mathematical treatment of the phenomena encountered in x-ray diffraction in crystals.

Chapter I starts with the macroscopic concept of a crystal and of crystal faces, introduces the lattice concept, the reciprocal lattice, and Fourier development of crystal properties.

Chapter II contains an excellent and concise discussion of the symmetry properties of crystals. Throughout the chapter dyadic algebra is used rather than geometric considerations. The properties of dyadics required, as well as the group theory needed, are derived in Appendix A and B. The possible symmetry operations in crystals are discussed. The properties of the 32 point groups are derived and discussed. All possible space groups are listed, and their complete derivation is treated.

Chapter III deals with x-ray diffraction in ideal crystals. The Laue and Bragg equations are deduced, and the construction of the diffracted vector discussed. The main part of the chapter is devoted to the calculation, from the atomic scattering power, of the intensity distribution in the interference maxima. Formulae are developed for the percent reflection, integrated scattering power, and half width in a number of cases. The cases treated are those of small crystals, thin, thick, and intermediate crystal plates, with and without absorption.

The agreement of these formulae with experiment is in general poor. The theory predicts smaller integrated intensity and narrower intensity distribution than those found experimentally at the Laue-Bragg spots. The reason for the difference is to be found in the crystal imperfections.

These imperfections are taken up in Chapter IV, where the discrepancy between experiment and theory is resolved. The mosaic structure of crystals is shown to be able to account for the broader and more intense interference maxima which are observed. Another important disorder is the heat motion. The normal coordinates of the lattice are introduced, and their thermal vibrations are shown to give rise to diffuse scattering and a decrease of intensity of the interference maxima. Temperature motion taken alone, without the imperfections due to mosaic structure, would increase the disagreement between theory and experiment. The last section discusses some common disorders found in real crystals.

The book is clearly and concisely written throughout. All the material in it is completely and logically derived from the fundamental concepts. The numerous formulae for intensity and half width ought to be very useful for a worker in the field. A considerable amount of the material of the book consists in original work of the author and cannot be found in any publication. This is especially true of the treatment of mosaic structure in Chapter IV.

The book is extensively mathematical. Dr. Zachariasen ends his introduction with the sentence: "The modest size of this book is not a fair measure of the time I have spent on it." This is indeed to be believed. The reader trying to master the material of this book may find the same statement to apply to himself.

MARIA GOPPERT MAYER
Dept. of Chemistry
Columbia University

PYRITES DEPOSITS OF MISSOURI by Oliver R. Grawe has recently been issued as volume 30 of the *Missouri Geological Survey and Water Resources*. This report of 482 pages describes the location, history, geologic conditions and production of 91 mines and prospects. Spectrographic analyses of the pyrites and its oxidation products have shown the presence of 23 elements, most of which are present in amounts less than 0.05%. The report also includes *x*-ray analyses, studies of polished sections and a description of 36 minerals that have been reported as occurring in the pyrites and iron ore bearing sink structures of the northern Ozark plateau.

REPORT OF INVESTIGATIONS NO. 50 OF THE SOUTH DAKOTA GEOLOGICAL SURVEY embraces a "Preliminary Report on the Mineralogy of some Pegmatites near Custer" by D. Jerome Fisher. The main object is to suggest an economical plan for the recovery of the valuable minerals in the pegmatites of the area. This report covers the history, geology, detailed mineralogy and paragenesis of five pegmatites designated by the following Lodes: Buster, Earl, Custer Mountain, Old Mike and Ross. Descriptions of the geology of three of the pegmatites of the Custer District appear in Report of Investigations No. 44 of the South Dakota Geological Survey.

PHILADELPHIA MINERALOGICAL SOCIETY

Academy of Natural Sciences of Philadelphia, May 5, 1945

Dr. W. Hersey Thomas presided, with 59 present. Dr. Hugh E. McKinstry of the Foreign Economic Administration addressed the society on "Collecting minerals for the war." Sources of mica, beryl, iceland-spar, vanadium and tungsten were described.

Meeting of June 7, 1945

Dr. Thomas was in the chair, with 54 present. Dr. William J. Kirkpatrick addressed the members on "Growth of Crystals." The historical introduction to the growth of euhedral crystals included Robert Boyle's (1669) observation that the rate of growth influences crystal habit, Romé Delisle's (1783) observation that sodium chloride crystallizes in octahedra from urine, and Le Blanc's (1808) observation that alum is octahedral when grown in weak alkali solutions. Beudant (1818) published a paper of 100 pages on the causes that determine the variations of crystalline forms.

Some factors that influence crystal habit are *p*H of a solution, presence of cosolutes, colloids or dispersing agents, rate of growth, temperature, pressure, and degree of agitation. A law of crystal growth may be stated: "If all of the faces grow at the same rate, the faces will disappear in the order of their distance from the center, $d=1/\sqrt{h^2+k^2+l^2}$, where h, k, and l are the Miller indices.

Sodium chloride usually crystallizes in cubes; the presence of urea and other alkalies in the solution cause it to crystallize in striated octahedra, although no record could be found of anyone having obtained good reflections on the goniometer from octahedral faces.

Some practical applications of crystal habit control were given: the dodecahedral face is the most effective plane in nickel for catalyzing hydrogenation reactions. Because they dissolve at a predetermined rate, many commercial chemicals such as photographer's hypo and sodium chromate are supplied in uniform equidimensional crystals. The habit of cupric chloride is influenced by the presence of certain tissue extracts: a fact made use of in pathology.

J. S. Frankenfield, *Secretary.*

NEW YORK MINERALOGICAL CLUB, INC.

Abstract of Meeting of May 16, 1945

The president and treasurer gave their annual reports and a trip to the William Boyce Thompson collection was announced. Mr. Newton Marshall, Vice-president of the South American Gold and Platinum Co. described dredging operations for precious metals in the Choco region of South America, illustrating his lecture with a motion picture.

ELIZABETH ARMSTRONG, *Secretary.*

Abstract of Meeting of October 17, 1945

With an attendance of about eighty, the New York Mineralogical Club opened its fall season with the usual meeting on summer collecting by members. In spite of the difficulties of travel members managed to visit New Mexico, Colorado, Pennsylvania, New York, New Hampshire, Maine, Vermont, Connecticut, New Jersey, and Massachusetts localities with the usual varying degrees of success. The most notable finds were 18 faceted beryl crystals, good New Jersey carnelian, Connecticut green gem tourmalines, and minerals from St. Peter's Dome, Colorado.

Mrs. E. J. MARCIN, *Secretary.*

NEW MINERAL NAMES

Alumino-chrysotile

D. P. SERDYUCHENKO: Alumino-chrysotile, a member of the isomorphous series serpentine-parakaolinite. *Compt. rend. acad. sci. U.R.S.S.*, **46**, 117–118 (1945).

Flattened-columnar green chrysotile, with fibers 15–20 cm. in length, was found in the basin of the Markopidj River, North Caucasus. Analysis gave: SiO_2 42.54, Al_2O_3 5.68, Fe_2O_3 1.06, FeO 0.74, MgO 35.57, CaO 0.13, H_2O- 0.38, H_2O+ 13.26; sum 99.36%. This corresponds to 87% chrysotile, 13% kaolinite. The mineral occurs at the contact of granite with serpentinites.

DISCUSSION: An unnecessary name for aluminian chrysotile.

MICHAEL FLEISCHER.

Unnamed

ANDERS BYSTRÖM: Monoclinic magnetic pyrites. *Arkiv. för Kemi, Mineral. Geol.*, **19B**, No. 8, 1–8 (1945).

X-ray study was made of 19 pyrrhotite samples from Swedish localities. Five were found to be hexagonal, with $a = 3.434$ to $3.437 \pm .002$ Å, $c = 5.714$ to $5.726 \pm .003$ Å. Three samples were analyzed for S giving 51.93, 53.03 and 53.20 atomic % S. Ten samples were found to be monoclinic, with $a = 5.933$ to 5.941 Å, $b = 3.425$ to 3.430, $c = 5.677$ to 5.689 Å, $\beta = 89.56°$ to 89.64°. Nine samples were analyzed for S, giving 51.74 to 53.01 atomic % S. Four samples were found to be mixtures of the hexagonal and monoclinic forms. A sample of the monoclinic mineral and one of the mixtures were transformed into hexagonal phases when heated for 15 hours at 600°C. in evacuated quartz tubes.

M.F.

INDEX TO VOLUME 30

Leading articles are in **bold face** type; notes, abstracts and reviews are in ordinary type Only minerals for which definite data are given are indexed.

Ahrens, L. H. Quantitative spectrochemical examination of minor constituents in pollucite 616

Alumino-chrysotile (Serdyuchenko) 724

Amphiboles, calciferous, variations in composition and properties of. (Winchell) 27

Arellano, A. R. V. Platinum crucible substitutes under war limitations 540

Baker, G. Eclogite inclusion from Cape Patterson volcanic neck in South Gippsland, Victoria .. 505

Banalsite (Smith, Bannister, Hey). 85

Bannister, F. A. 85

Barthite = austinite (Fischer) 550

Bastnäsite (Glass, Smalley) 601

Bateman, J. D. Composition of Bird River chromite, Manitoba 596

Bayramgil, O. 86

Berman, Harry, memorial of. (Hurlbut) 124

Borosilicate occurrence in diabase at Lambertville, N. J. (Tomlinson) 203

Bradley, W. F. Diagnostic criteria for clay minerals 704

Brazilianite, a new phosphate mineral. (Pough, Henderson) 572

Buerger, M. J. Genesis of twin crystals 469

——— **Soap crystals** 551

——— Photography of the reciprocal lattice. [Book review] 83

Buie, B. F. with Van Valkenburg, A. Octahedral cristobalite with quartz paramorphs from Ellora Caves, Hyderabad, India. 526

Butler, R. D. with Stoiber, R. E. and Tolman, C. Geology of quartz crystal deposits 245

Bryström, A. 724

Calogerasite = simpsonite (Guimaraens) 549

Cattierite and vaesite; new Co-Ni minerals from Belgian Congo. (Kerr) 483

Celestite from Livingston Co., Ky. (Harden, Thurston) 639

Cement-aggregate reaction in concrete (McConnell, Irwin) 78

Cerium and columbium minerals in Montana. (Cooke, Perry) .. 623

Chromite, Bird River, Manitoba, composition of. (Bateman) ... 596

Clay minerals, diagnostic criteria for. (Bradley) 704

Cloos, E. Memorial of Edward B. Mathews 135

Cogswell, R. F. Hollow prism for goniometric calibration of refractive index media 541

Columbium and cerium minerals in Montana. (Cooke, Perry) 623

Cooke, S. R. B. and Perry, E. S. Columbium and cerium minerals in Montana 623

Copper and silver sulfide minerals in polished sections, localization of, by KCN etch pattern. (Yagoda) 51

Cristobalite, octahedral, with quartz paramorphs from Ellora Caves, Hyderabad State, India. (Van-Valkenburg, Buie) 526

Cristobalite from Ellora Caves, India, crystallography of. (Wolfe) 536

Cutting schemes for quartz crystals. (Gordon, Parrish) 347

Dauphiné twinning, secondary, in quartz. (Frondel) 447

de Villiers, J. E. Lithiophorite from Postmasburg manganese deposits 629

Dictionary of Gems and Gemology. (Shipley, Beckeley, Wigglesworth Shipley) [Book review]. 545
Dihydrite from Mineral Co., Nevada. (Goudey) 640
Discredited minerals 550
Donnay, J. D. H. Destruction of Liegé Museum 81

Eclogite inclusion from Cape Patterson volcanic neck in South Gippsland, Victoria. (Baker) 505
Effect of imperfections on usability of quartz for oscillator-plates. (Lukesh) 291
Emmons, R. C. A mineralogist's obligation 87
——— Nepheline syenites of Wausau, Wisconsin 169
English, George L., memorial of. (Vance) 130
Error, maximum, in some mineralogic computations (Fairbairn, Sheppard) 673

Fackler, W. C. Occurrence of nemalite in Alaska 640
Fahey, J. Memorial of George Steiger 153
Fairbairn, H. W. and Sheppard, C. W. Maximum error in some mineralogic computations 673
Faust, G. T. Book review 545
Final frequency adjustment of quartz oscillator-plates. (Frondel) 416
Fischer, E. 550
Fisher, D. J. Preliminary report of mineralogy of some pegmatites near Custer 723
Florida beach and dune sands, heavy minerals of. (Miller) 65
Formulas for fine grained minerals, calculating on basis of chemical analysis. (Kelley) 1
Frondel, C. Effect of radiation on elasticity of quartz 432
——— **Final frequency adjustment of quartz oscillator-plates** 416
——— **History of quartz oscillator-plate industry** 205
——— **Secondary Dauphiné twinning in quartz** 447

Glass, J. J. and Smalley, R. G. Bastnäsite 601
Glossary of terms used in quartz oscillator-plate industry 461
Gordon, S. G. Inspection and grading of quartz 269
——— 543, 550
——— **and Parrish, W. Cutting schemes for quartz crystals** 347
——— **Orientation techniques for manufacture of quartz oscillator-plates** 296
——— **Precise angular control of quartz-cutting by x-rays** 326
Goudey, H. Dihydrite from Mineral Co., Nevada 640
Gramling-Mende, I. 548
Grawe, O. R. Book review 723
Groutite, $HMnO_2$, a new mineral of the diaspore-goethite group. (Gruner) 169
Gruner, J. W. Groutite, a new mineral of the diasporegoethite group 169
Guimaraens, C. P. 549

Handbook of mineral dressing, ores and industrial minerals. (Taggart) [Book review] 544
Hardin, G. C., Jr., and Thurston, W. R. Celestite from Livingston Co., Ky. 639
Hedleyite. (Warren, Peacock) 644
Helvite from western Australia, refractive index of 204
Henderson, E. P. with Pough, F. H. Brazilianite, a new phosphate mineral 572
Hey, M. H. 85
History of quartz oscillator-plate industry 1941-4. (Frondel) 205
Hollow prism for goniometric calibration of refractive index media. (Cogswell) 541
Holmes, R. J. and Knox, M. S. with Kerr, P. F. Lattice constants in the pyrite group 498
Hubbard, B. Observations on opti-

cal properties of long chain normal paraffins 645
Hunt, W. F. Presentation of Roebling Medal to E. H. Kraus . . . 111
Hurlbut, C. S. Jr. Memorial of Harry Berman 124
Hutton, C. O. Additional optical and chemical data on stilpnomelane group 714

Inspection and grading of quartz. (Gordon) 269
Indium, occurrence and hardness of. (McLellan) 635
Irwin, W. H. with McConnell, D. Cement-aggregate reaction in concrete 78

Justite (Gramling-Mende, Leopold) 548

Kelley, W. P. Calculating formulas for fine grained minerals on basis of chemical analysis 1
Kerr, P. F. Cattierite and vaesite; new Co-Ni minerals from Belgian Congo 483
——— Holmes, R. J. and Knox, M. S. Lattice constants in the pyrite group 498
Knoop microhardness tester as a mineralogical tool. (Winchell) 583
Knox, M. S. with Kerr, P. F. and Holmes, R. J. Lattice constants in the pyrite group 498
Kraus, E. H. Acceptance of the Roebling Medal 115
——— Book review 545

Lattice constants in the pyrite group. (Kerr, Holmes, Knox). 498
Leopold, G. 548
Liegé Museum, destruction of 81, 538
Lithiophorite from Postmasburg manganese deposits. (deVilliers) 629
Lithiophorite, chemical analysis (van der Walt) 631
Lovering, T. S. and Stringham, B. Zunyite in Utah 76
Lukesh, J. S. Effect of imperfections on usability of quartz for oscillator-plates 291

Machine lapping of quartz oscillator-plates. (Parrish) 389
Magne, A. 86
Mathews, Edward B., memorial of. (Cloos) 135
Mayer, M. G. Book review 722
McConnell, D. and Irwin, W. H. Cement-aggregate reaction in concrete 78
McLellan, R. D. Occurrence and hardness of indium 635
Mélon, J. 548
Metavauxite, crystallographic data and chemical analysis 550
Methods and equipment for sawing quartz cyrstals. (Parrish) 347
Miller, Benjamin L., memorial of. (Stewart) 142
Miller, R. Heavy minerals of Florida beach and dune sands 65
Mineralogic computations, maximum error in. (Fairbairn, Sheppard) 673
Mineralogical Society of America:
  Announcement of annual meeting 643
  List of correspondents, fellows and members 177
  List of suscribers 194
  Nominations for officers for 1946 642
  Proceedings for 1944 169
Mineralogist's obligation. (Emmons) 87
Montmorillonite (Winchell) 510
Murdoch, J. Probertite from Los Angeles Co., Calif. 719
Myers, W. M. Book review 544

Nemalite occurrence in Alaska (Fackler) 640
Nepheline syenites of Wausau, Wisconsin (Emmons) 169
New minerals described:
  Brazilianite 572
  Cattierite 483
  Vaesite 483
New mineral names 85, 548, 644, 724
New York Mineralogical Club 85, 547, 724

Optical properties of organic compounds. (Winchell) [Book re-

view] 545
Orientation techniques for manufacture of quartz oscillator-plates. (Parrish, Gordon) 296

Paraffins, long chain normal, optical properties of. (Hubbard) . . 645
Paravauxite, chemical analysis 550
Parrish, W. Machine lapping of quartz oscillator-plates 389
——— **Methods and equipment for sawing quartz crystals** 371
——— **and Gordon, S. G. Cutting schemes for quartz crystals** . . . 347
——— **Orientation techniques for manufacturing quartz oscillator-plates** 296
——— **Precise angular control of quartz-cutting by x-rays** 326
Parsons, A. L. Memorial of Joseph E. Thomson 157
Peacock, M. A.. 644
Pegmatites near Custer, mineralogy of. (Fisher) 723
Perry, E. S. with Cooke, S. R. B. Columbium and cerium minerals in Montana 623
Philadelphia Mineralogical Society 84, 548, 723
Photography of the reciprocal lattice. (Buerger) [Book review] . 83
Piezoelectric quartz resonator. (Van Dyke) 214
Platinum crucible substitutes under war limitations. (Arellano) 540
Pollucite, quantitative spectrochemical examination of minor constituents in. (Ahrens) 616
Pough, F. H. and Henderson, E. P. Brazilianite, a new phosphate mineral 572
Precise angular control of quartz cutting by x-rays. (Parrish, Gordon) 326
Probertite from Los Angeles Co., California (Murdoch) 719
Pseudoapatelite (Magne) 86
Pyrite group, lattice constants in. (Kerr, Holmes, Knox) 498
Pyrites deposits of Missouri. (Grawe) [Book review] 723
Pyrites, monoclinic magnetic (Byström) 724

Quartz crystal deposits. geology of. (Stoiber, Tolman, Butler) 245
Quartz oscillator-plates, symposium on 205–461

Radiation, effect of, on elasticity of quartz. (Frondel) 432
Ramsdell, L. S. Crystal structure of α-SiC, type VI 519
——— Book review 83
Roebling Medal:
Presentation to E. H. Kraus. (Hunt) 111
Acceptance. (Kraus) 115

Schaller, W. T. Memorial of Frank C. Schrader 148
——— **Memorial of Roger C. Wells** 163
Schrader, Frank C., memorial of. (Schaller) 148
Serdyuchenko, D. P. 724
Sheppard, C. W., with Fairbairn, H. W. Maximum error in some mineralogic computations 673
Shipley, R. M. Dictionary of Gems and Gemology. [Book review]. 545
Silicon carbide (α), type VI, crystal structure of, (Ramsdell) 519
Smalley, R. G., with Glass, J. J. Bastnäsite 601
Smith, W. C. 85
Soap crystals. (Buerger) 551
Steiger, George, memorial of. (Fahey) 153
Steiger, J. v. 86
Stewart, D., Jr. Memorial of Benjamin L. Miller 142
Stilpnomelane group, additional optical and chemical data on. (Hutton) 714
Stoiber, R. E., Tolman, C. and Butler, R. D. Geology of quartz crystal deposits 245
Stringham, B., with Lovering, T. S. Zunyite in Utah 76
Symposium on quartz oscillator-plates 205-461

Taggart, A. F. Handbook of mineral dressing, ores and industrial minerals. [Book review] 544

Theory of x-ray diffraction in crystals. (Zachariasen) [Book review] 722

Thomson, Joseph E., memorial of. (Parsons) 157

Thurston, W. R., with Hardin, G. C. Celestite from Livingston Co., Ky. 639

Tin mines of Cerro de Llallagua, Bolivia. (Gordon) 543

Tolman, C. and Butler, R. D. with Stoiber, R. E. Geology of quartz crystal deposits 245

Tomlinson, W. H. Occurrence of borosilicates in diabase at Lambertville, N. J. 203

Tungsten deposit near Townsville, N. C. (White) 97

Twin crystals, genesis of. (Buerger) 469

Vaesite and cattierite: new Co-Ni minerals from Belgian Congo. (Kerr) 483

Vance, R. C. Memorial of George L. English 130

van der Walt, C. F. J. Chemical analysis of lithiophorite 631

Van Dyke, K. S. Piezoelectric quartz resonator 214

Van Valkenburg, A. and Buie, B. F. Octahedral cristobalite with quartz paramorphs from Ellora Caves, Hyderabad, India 526

Vauxite, crystallographic and chemical data 550

Viseite (Mélon) 548

Warren, H. V. 644

Wells, Roger C., memorial of. (Schaller) 163

White, W. A. Tungsten deposit near Townsville, N. C. 97

Winchell, A. N. Montmorillonite . . 510

——— Variations in composition and properties of calciferous amphiboles 27

——— Optical properties of organic compounds. [Book review] 545

Winchell, H. Knoop microhardness tester as a mineralogical tool 583

Wolfe, C. W. Crystallography of cristobalite from Ellora Caves, India 536

Yagoda, H. Localization of Cu and Ag sulfide minerals in polished sections by KCN etch pattern. 51

Yenerite (Steiger, Bayramgil) 86

Zachariasen, W. H. Theory of x-ray diffraction in crystals. [Book review] 722

Zunyite in Utah. (Lovering, Stringham) 76